Effect of Device Design on the Performance of a Dry Powder Inhaler

Using Computational Fluid Dynamics

Tan   Suwandecha

A Thesis Submitted in Partial Fulfillment of the Requirements for the Degree of

Doctor of Philosophy in Pharmaceutical Sciences

Prince of Songkla University

2014

Thesis Title   Effect of Device Design on the Performance of a Dry
Powder Inhaler Using Computational Fluid Dynamics

Author   Mr. Tan Suwandecha

Major Program   Pharmaceutical Sciences

Major Advisor   **Examining Committee:**

…………………………..……………..

(Assoc. Prof. Dr. Teerapol Srichana)

………………………………..…….Chairperson

(Assoc. Prof. Dr. Pruittikorn Smithmaitrie)

Co-advisor

………………………………………………..

(Assoc. Prof. Dr. Teerapol Srichana)

…………………………………………....

(Assoc. Prof. Wibul Wongpoowarak)

………………………………………..…………

(Assoc. Prof. Wibul Wongpoowarak)

…………………………….………...…………

(Dr. Chonladda Pitchayajittipong)

The Graduate School, Prince of Songkla University, has approved this thesis as partial fulfillment of the requirements for the Degree of Doctor of Philosophy in Pharmaceutical Sciences.

………………………………..………..

(Assoc. Prof. Dr. Teerapol Srichana)

Dean of Graduate School

This is to certify that the work here submitted is the result of the candidate's own investigations. Due acknowledgement has been made of any assistance received.

…………………………………....

(Assoc. Prof. Dr. Teerapol Srichana)

Major Advisor

…………………………………..

(Mr. Tan Suwandecha)

Candidate

I hereby certify that this work has not already been accepted in substance for any degree and is not being concurrently submitted in candidature for any degree.

…………………………………..
(Mr. Tan Suwandecha)
Candidate

ชื่อวิทยานิพนธ์	การออกแบบอุปกรณ์นำส่งยาต่อประสิทธิภาพยาสูดแบบผงแห้งโดยใช้การคำนวณจลนศาสตร์ของไหล
ผู้เขียน	นายธันว์ สุวรรณเดชา
สาขาวิชา	เภสัชศาสตร์
ปีการศึกษา	2557

บทคัดย่อ

การนำส่งยาสู่ทางเดินหายใจมีข้อดีหลายประการเช่น ทำให้ยาออกฤทธิ์ได้เร็ว มีประสิทธิผลดี และลดอาการข้างเคียงของยา ยาสูดชนิดผงแห้ง (Dry powder inhalers) เป็นรูปแบบการนำส่งยาเข้าสู่ทางเดินหายใจที่มีการศึกษาวิจัยกันอย่างแพร่หลาย แต่ประสิทธิภาพการนำส่งยายังไม่ดีนัก อนุภาคยาส่วนมากไม่สามารถลงไปสู่ทางเดินหายใจส่วนล่างได้ อุปกรณ์นำส่งยาเป็นส่วนสำคัญที่ส่งผลต่อประสิทธิภาพการนำส่งยา กลไกการไหลของอากาศ และอันตรกิริยาระหว่างอนุภาคในอุปกรณ์นำส่งยาชนิดผงแห้งมีผลอย่างมากต่อกระบวนการกระจายตัวของผงยา การศึกษากลไกทางกลศาสตร์ของไหล และการชนกันของอนุภาค จึงเป็นแนวทางสำคัญในการปรับปรุงอุปกรณ์นำส่งยาสูดชนิดผงแห้ง งานวิจัยชิ้นนี้ได้ศึกษากระบวนการกระจายตัวยาสูดชนิดผงแห้งในอุปกรณ์ Cyclohaler® และ Inhalator® โดยใช้การจำลองจลนศาสตร์ของไหลด้วยคอมพิวเตอร์ (Computational fluid dynamics) ตัวแปรที่สนใจคือพลังงานจลน์ของการไหลแบบปั่นป่วน (Turbulent kinetic energy) และการชนของอนุภาคผงยากับผนังอุปกรณ์นำส่งและดัดแปลงอุปกรณ์ Cyclohaler® ด้วยกระบวนการออกแบบด้วยคอมพิวเตอร์ (Computer aided design) และการสร้างตัวอย่างอย่างรวดเร็ว (Rapid prototyping) เพื่อสร้างอุปกรณ์นำส่งยาสูดชนิดผงแห้งที่มีประสิทธิภาพสูงขึ้น การประเมินประสิทธิภาพของการนำส่งยาภายนอกร่างกายทำด้วย Andersen cascade impactor โดยใช้สูตรตำรับ Salbutamol Sulfate ที่มีขนาดตัวพาต่างๆ กัน และสูตรตำรับที่มีจำหน่ายในทาง

การค้า Ventolin Rotacaps® การทดลองพบว่าการไหลของอากาศใน Cyclohaler® เป็นการไหลแบบหมุนวนในส่วนต้นของอุปกรณ์ และเมื่อผ่านตะแกรงจะไหลเป็นแนวตรงมากขึ้น ส่วนการไหลใน Inhalator® นั้นอากาศจะไหลเป็นลักษณะเส้นตรงไปตามความยาวของอุปกรณ์ พลังงานจลน์การไหลแบบปั่นป่วนแปรผันโดยตรงกับอัตราการไหลของอากาศในอุปกรณ์ Cyclohaler® และ Inhalator® โดยที่พลังงานจลน์ของการไหลแบบปั่นป่วนใน Cyclohaler® มีค่าน้อยกว่าใน Inhalator® เนื่องจาก Inhalator® มีช่องทางไหลของอากาศแคบกว่าทำให้อากาศมีความเร็วสูง นอกจากนี้ยังพบว่าปัจจัยที่ส่งผลต่อการแตกตัวของกลุ่มอนุภาคโดยการชนคือการไหลแบบหมุนวนใน Cyclohaler® และตะแกรงใน Inhalator® อย่างไรก็ตาม Inhalator® มีความต้านทานการไหลของอากาศสูงอาจจะมีผลให้ผู้ป่วยสูดหายใจผ่านอุปกรณ์ได้ยาก จึงเลือกที่จะดัดแปลง Cyclohaler® ผสมผสานกับ Rotahaler® ที่มีความต้านทานการไหลต่ำแทน อุปกรณ์ที่สร้างขึ้นใหม่มี 3 รูปแบบ แตกต่างกันที่ตำแหน่งตะแกรง และขนาดช่องทางไหลของอากาศ การทดลองพบว่า อุปกรณ์ทั้ง 3 แบบและ Cyclohaler® มีค่าสัดส่วนอนุภาคละเอียด (Fine particle fraction) 23%, 36%, 50% และ 35% ตามลำดับ อุปกรณ์รูปแบบที่ 3 สามารถให้สัดส่วนอนุภาคละเอียดสูงที่สุด ส่วนอุปกรณ์รูปแบบที่ 2 และ Cyclohaler® ให้สัดส่วนอนุภาคละเอียดในระดับเดียวกัน และอุปกรณ์รูปแบบที่ 1 ให้สัดส่วนอนุภาคละเอียดน้อยที่สุด โดยสรุปแล้วกลไกการกระจายตัวของยาสูดชนิดผงแห้งขึ้นกับพลังงานจลน์ของการไหลแบบปั่นป่วน และการชนของอนุภาคผงยากับผนังอุปกรณ์นำส่ง โดยทั้งสองปัจจัยมีความสำคัญเท่าเทียมกัน และอุปกรณ์รูปแบบที่ 3 เป็นรูปแบบที่จะใช้ในการพัฒนาต่อไปเพื่อ ให้ใช้ในผู้ป่วยจริงได้อย่างสะดวกและปลอดภัย

Thesis Title	Effect of Device Design on the Performance of a Dry Powder Inhaler Using Computational Fluid Dynamics
Author	Mr. Tan Suwandecha
Major Program	Pharmaceutical Sciences
Academic Year	2014

Abstract

Pulmonary aerosol drug delivery has several benefits over the other routes for instance rapid onset, improve bioavailability and reduce side effects. Dry powder inhalers (DPIs) gain interesting in drug delivery researches. Though, it is not able to produce high fine particle fractions that reach the lower parts of lungs. DPIs device is an important factor that determine the performance of the DPIs system. The different in DPIs design changes the dynamic processes that the airflow interacts to the dry powder particles and also particles - device wall interaction. The dynamic processes in the device changes the aerosol dispersion performance. Therefore, investigation of the processes involves the airflow and the particles impaction dynamics are important step in the DPIs device development. The Cyclohaler® and the Inhalator® were selected as the commercially available devices in this research. The fluid dynamics behaviors were observed using computational fluid dynamics (CFD). Turbulence kinetic energy (TKE) and particles - device impaction related parameters were investigated. New inhalers devices were designed using computer aided design (CAD). The prototypes of the proposed inhaler devices were created using rapid prototyping machine. The model DPIs formulations were salbutamol sulfated blended with 3 sizes of lactose carriers and a commercially available formulation, Ventolin

Rotacaps®. It was observed that the airflow in the Cyclohaler® was a swirly flow at the capsule chamber of the inhaler. The airflow was regulated by a grid to a straight flow along the mouthpiece. On the other hand, the airflow in the Inhalator® was straightened and aligned to the longitudinal length of the inhaler. The TKE was dramatically stronger in the Inhalator® than that occurred in the Cyclohaler® because of the Inhalator® internal geometry was narrow and generated high airflow velocity. The most important factors that affected the DPI particles-device impaction were swirly flow in the Cyclohaler® and the grid in the Inhalator®. These designs were chosen as starting references for new DPIs. However the Inhalator® had very high airflow resistance that could be an obstacle for asthmatic exacerbated patients who have low inhalation power. Thus, the new DPIs designs were based on the Cyclohaler® and the Rotahaler®. The Rotahaler® grid and mouthpiece parts and the Cyclohaler® cyclonic chamber were modified to form 3 new DPIs designs. The new designs were different in grid position and mouthpiece size. The aerosol dispersion experiment revealed that fine particles fraction (FPF) in Cyclohaler® and the 3 DPIs models were 35%, 23%, 36% and 50%, respectively. The proposed inhaler model 3 device generated the highest FPF among the 4 devices. The proposed inhaler model 2 device and the Cyclohaler® had no statistical difference in the FPF. Whereas the proposed inhaler model 1 device generated the poorest FPF. In summary, the DPIs device performance depended on the turbulence based factor and the dry powder particles-device impaction factor. Both factors had similar significant level. The proposed inhaler model 3 device was the best design in this research. It was chosen for further development to optimize usability and cost effectiveness.

ACKNOWLEDGEMENT

This Ph.D. thesis was success by the author and the cooperation of many people. They provided not only academic contributions, but also some social supportive. Therefore I would like to thank everyone who contributed to this thesis.

First of all, I would like to thank my major advisor, **Associate Professor Dr. Teerapol Srichana**, Faculty of Pharmaceutical Sciences, Prince of Songkla University and Dean of Graduate School, Prince of Songkla University, who give me the inspiration of this Ph.D. thesis. He also pays attention not only to my work but also all of his post-graduate students. I would like to gratefully and sincerely thanks to my co-advisor, **Associate Professor Wibul Wongpoowarak** Faculty of Pharmaceutical Sciences, Prince of Songkla University, who suggests about mathematics and statistical analysis. I extended my thank to **Dr. Kittinan Maliwan**, Department of Mechanical Engineering, Faculty of Engineering, Prince of Songkla University who advised in computational fluid dynamic theory.

I would like to thank Department of Pharmaceutical Technology, Faculty of Pharmaceutical Sciences, Prince of Songkla University for supporting facilities and research materials. I also extended my thanks to Center of Excellence in Nanotechnology for Energy, **Associate Professor Dr. Pruittikorn Smithmaitrie**, **Associate Professor Dr. Nantakan Muensit, Mr. Ugrit Chammari and Mr. Krit Koyvanich** for supporting rapid prototyping machine. I also appreciated Nanotec-PSU Excellence Center on Drug Delivery System, Faculty of Pharmaceutical Sciences, Prince of Songkla University for extensively supporting facilities. Also go to all staff and scientists from this center (**Ms. Titpawan Nakpheng**, **Ms. Wilaiporn Buatong**, **Mr. Ekawat Thawithong**, **Mr. Vikrom Changsarn**, and **Ms. Kornkamon Petyord**) for training me to operate the equipment and supported me in my research work. I thank them for all of their help. I have to also acknowledge all good friends of Ph.D. and M. Pharm. students during my study period, **Mr. Somchai Sawasdee**, **Mr. Janwit Dechraksa**, **Ms. Anongtip S.A.**, **Ms. Kanogwan Keawjan**, and **Ms. Teerarat Rattanupatam**, for helping and discussion some works. I also

appreciative to thanks **Dr. Brian Hodgson** for editing of the manuscript and offering suggestions for English language. I have to express and forever grateful the profound appreciation to **my parents** for encouragement, inspiration and support me in all my life.

The author alone assumes responsibility for discussion and conclusions of this thesis and any errors of it may contain.

Lastly, the most special thanks go to all readers.

Tan Suwandecha

CONTENTS

LIST OF TABLES

LIST OF FIGURES

LIST OF ABBREVIATIONS AND SYMBOLS

μm	micrometer
ACI	Andersen Cascade Impactor
CAD	computer aided design
CFD	computational fluid dynamics
COPD	chronic obstructive pulmonary disease
DEM	discrete element modelling
DPI	dry powder inhaler
FPF	fine particle fraction
GSD	geometric standard deviation
ISSR	integral scaled strain rate
HPLC	high performance liquid chromatography
MMAD	mass median aerodynamic diameter
nm	nanometer
NDSD	non-dimensional specific dissipation
P_{deagg}	probability of deagglomeration by impaction
pMDI	pressurized metered dose inhaler
SD	standard deviation
TI	turbulence intensity
TKE	turbulent kinetic energy

LIST OF PAPERS AND PROCEEDINGS

This thesis is based on the following papers, referred to their order of experimental design in the text. The publications are attached as appendices at the end of the thesis (from page 29 to 74). Reprinted are published with kind permission of the respective journals.

Paper 1   Suwandecha, T., Wongpoowarak, W., Maliwan, K., Srichana, T. 2014. Effect of turbulent kinetic energy on dry powder inhaler performance. *Powder Technology* 267:381-391.
Impact Factor (2013) : 2.269

Paper 2   Suwandecha, T., Wongpoowarak, W.,Srichana, T. Computer-aided design of dry powder inhalers using computational fluid dynamics to assess performance. *Pharmaceutical Development and Technology*. Published online 29 Sep 2014.
Impact Factor (2013) : 1.335

Proceedings 1   Suwandecha, T., Srichana, T., 2012. Aerodynamics Study in Dry Powder Inhalers Using Computational Fluid Dynamics. The 2nd Current Drug Development International Conference, 2-4 May 2012 Phuket, Thailand.

GENERAL INTRODUCTION

Asthma and chronic obstructive pulmonary diseases (COPDs) are the conventional therapeutic indications of pulmonary drug delivery system (Daniher and Zhu, 2008). However, the respiratory drug delivery technology is advanced beyond the conventional usage. The inhalation systemic drug delivery is a potential administration route since lungs have large absorption area for medicine. The total surface area of the lung is about 75 m^2. In addition, it improves bioavailability for many drugs due to bypass the hepatic first pass circulation. Recently peptides, proteins and hormones inhalation formulations were available (Grant and Leone-Bay, 2012, Kandasam and Chandrasekaran, 2013, Ramsey *et al.*, 2013).

The delivery of drug formulation to lungs associates with the physiology of human airways. The structure of human airways consists of multilevel cascade conducting tubes that branch from trachea to alveolar sacs. Diameter of airways duct serially decreases in each level of branching that affects to particle deposition pattern. The large particles deposit on upper level of airways while small particles can reach to alveolar area. From physiological limitation of airways, inhalation delivery system needs intensively optimization.

The pulmonary delivery system is classified into 3 types that are nebulizers, pressurized metered dose inhalers (pMDIs) and dry powder inhalers (DPIs). The nebulizer generates small liquid droplet from liquid dosage form by adding atomizing force into the liquid. Then the liquid droplets flow through the air stream and are inhaled by patients. The pMDI is liquid dosage form either solution or suspension with pressurized propellant in a canister. The pressurized propellant is an atomization force in the system. It pushes liquid formulation through a nozzle and generates

aerosols. DPIs are energized using patient inhalation efforts to disperse dry powder medication into fine aerosols. The DPIs have several benefits such as reliable, portable and chemical stability. A good delivery device is a key factor to guarantee reliably performance and patient compliance. The inhalers have to allow patients to produce sufficient airflow through the device. The airflow then disperses and breakups the dry powder agglomerates, and delivers a dose to the lungs as therapeutically effective fine particles. The airflow generated by inhalation directly determines particle velocity and hence the ease of which particle is deagglomerated.
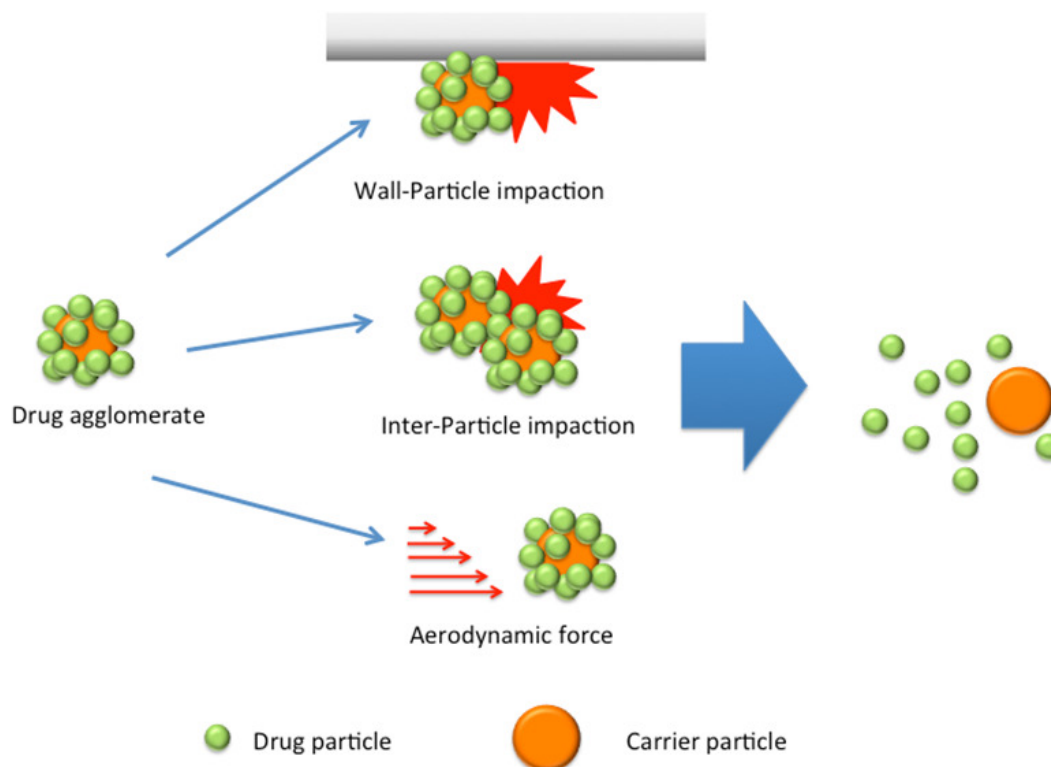
Figure 1 Dry powder aerosolization process.

The complex cascade physical aerodynamic processes were associated with the dry powder pulmonary delivery. The major processes are aerosolization of dry

powder, detachment of active drug particles from drug-only agglomerate or drug-carrier particle mixture, dispersion and transport of the aerosol through the target site in the airways (Islam and Cleary, 2012). The aerosolization processes involve with mechanical impaction either inter-particle impaction or particles – wall impaction and airflow shear force (**Figure 1**) (Zhou *et al.*, 2014). There are two approaches to maximize dry powder lung delivery: formulation optimizations and inhaler device design optimizations.

There are several methods for formulation optimizations such as nanoporous microparticles, hollow particles and multicomponent particles system. The particles are generated by spray drying, freeze drying, milling and spray freezing techniques (Depreter *et al.*, 2013, El-Gendy *et al.*, 2012, Hoppentocht *et al.*, 2014).

The DPIs formulation could be a drug powder only or a drug-carrier blend formulation. The carrier is usually lactose powder that acts as a bulk addition or diluent. The carrier is very large (30-110 μm) and is blended with only a few milligrams of the relatively smaller drug particles (less than 5 μm) (Karner *et al.*, 2014, Srichana *et al.*, 1998). The drug to carrier ratios can be varied such as 1: 67.5 (Diskhaler[®], Rotahaler[®] and Cyclohaler[®]), 1:4.6 (Pulmicort Flexhaler[®] 180 µg) and 1: 24 (Inhalator[®]) (AstraZeneca, 2010, Timsina *et al.*, 1994). The lactose carrier was known to improve the efficiency of drug delivery by reducing drug particle aggregations (Daniher and Zhu, 2008). The ternary or quaternary components are added in some formulations to optimize flow ability and dispersion efficiency. After aerosolization process in DPI device, the large carrier particles deposit on the upper airways, whereas the smaller drug particles reach the lower parts of the lungs (Zhou and Cheng, 2000).

The inhaler device design greatly influences the performance of the dry powder inhaler system. Over a dozen of dry powder inhalers are commercially available with various designs (Yang *et al.*). The design variation leads to differ in aerosol delivery performance. The DPI devices can be classified into three main types that are single unit dose, multiple unit dose and multiple dose (Cheng, 2014, Islam and Gladki, 2008). DPI formulation powder was precisely filled in individual capsule or blister pack in the single unit dose system (**Figure 2A**) (Daniher and Zhu, 2008). In the multiple unit dose system, formulation powder was also pre-fill in a blister pack, strip or wheel (**Figure 2B**) (Islam and Gladki, 2008). Both unit dose system and multiple units dose system provided protection of DPI formulation from environment moisture and reliable dosing accuracy from precisely dosing in the production process. The multiple dose devices incorporate bulk formulation powder reservoir and dosage metering mechanism (**Figure 2C**). It has benefit in term of easy handling of device and doesn't require manually unit dose changing. The drawback of the multiple dose devices is stability problem from moisture entering into the powder reservoir. Additionally, it is quite complicated to design the accurate and precise dosage metering mechanism (Islam and Cleary, 2012). From above information, the unit dose DPIs is simple and easier to design. Thus, the unit dose device is feasible to develop simple DPIs.

To develop efficient inhaler device, it is essential to understand factors affecting DPIs performance by studying from commercial available DPIs. Computational fluid dynamics (CFD) has been extensively used in the engineering researches. It is now increasing in popularity in aerosol delivery research (Coates *et al.*, 2006, Kleinstreuer and Zhang, 2003, Kleinstreuer *et al.*, 2008, Zhang *et al.*, 2004). CFD numerically solves the complex set of partial differential equations to represent the fluid

dynamics laws and simulates the fluid flow (Anthony and Flynn, 2006). The trend of dry powder inhaler device development is combination of the CFD and conventional experiment.

A: single unit dose   B: multiple unit dose   C: multiple dose
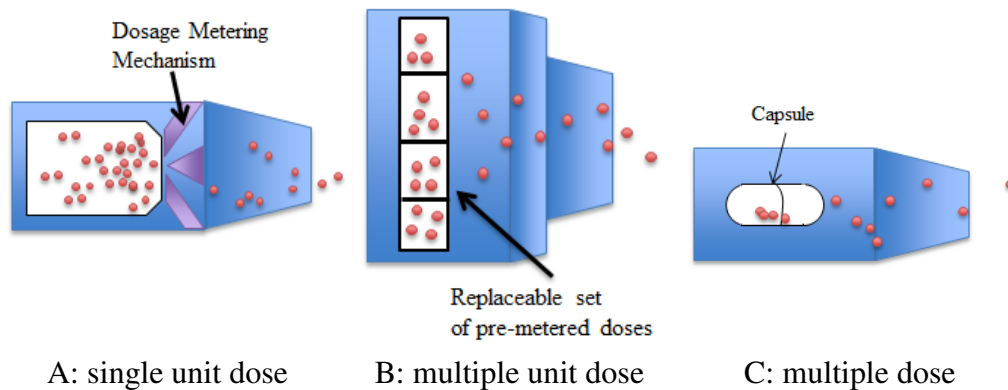
Figure 2 Single unit dose, multiple unit dose and multiple dose dry powder inhalers (Modified from Daniher and Zhu (2008))

There are several factors affecting the aerodynamic characteristic. A major factor is the degree of the turbulent flow in the inhalers. The degree of the turbulent flow and shear force in the device is directly related to the resistance of the device (Selvam *et al.*, 2010). An example of highly turbulence-based device is 3M Conix™. It is reverse cyclone design that creates high velocity swirly flow in the device. Previous CFD studies were described effect of air inlet size, grid structure and mouthpiece length of Aerolizer® device on dispersion performance using drug particles only model (Coates *et al.*, 2007). The grid structure in Aerolizer® aimed to increase fine particles fraction (FPF). However integral scale strain rate observation in CFD failed to explain relationship with FPF. The integral scale strain rate is derived from turbulent parameters. In this case, impaction potential of particles to device wall had combined

effects to integral scale strain rate on particles deagglomeration. In addition, grid structure contributed to regulate chaotic airflow to more laminar liked flow that reduce amount of device powder retention. In addition, the inhaler performance was scarcely related to the length of the mouthpiece when compared to the grid due to no statistically different in the performance of the inhaler was observed as the length of the mouthpiece was altered (Coates *et al.*, 2004, Coates *et al.*, 2006, Coates *et al.*, 2007).

Devices with high resistance usually provide a high degree of turbulence and shear force but can cause difficulty for asthmatics patient who have a limited inhalation force (Lee *et al.*, 2009). Turbuhaler™ is high resistant device with narrow spiral air flow channel to assist turbulence generation (Milenkovic *et al.*, 2013). The level of turbulence and particle collisions is influenced by the air inlet channel while the design of the mouthpiece controls the outlet air velocity and flow pattern (Gac *et al.*, 2008). The flow pattern in the device and the outlet air velocity may cause drug loss in the oropharyngeal region by inertial impactions (Ball *et al.*, 2008). One study has indicated how the dispersion capability of DPIs can be optimised by adjusting the magnitude of the turbulence and maximising the particle impaction velocity whereas the effect of the mechanical impaction on the dispersion of the particles is still unclear (Voss and Finlay, 2002). An experiment revealed that the particle and device wall impaction dominated in powder dispersion mechanism (Wong *et al.*, 2010). The conflict results leaded to another attempts to explain the effect of the fluid dynamics parameters to the DPIs performance. The non-dimensional specific dissipation (NDSD) was investigated to forecast dispersion performance in carrier-free DPI devices. The NDSD was classified in to 3 categories, flow-based factor, turbulence based factor and particles based factor. The flow-based factors were pressure drop and flow-rate. The

turbulence-based factors were TKE and turbulence intensity (TI). The particles based factors were wall impaction count and average trajectory integral. The correlation between the flow-based factor and dispersion performance was very weak. Thus, it is not appropriate to predict the dispersion performance. The turbulence-based factors such as TKE and particles-based factors were not well predicted MMAD (Longest *et al.*, 2013).

The advancement in computational analysis enabled the dynamically simulation of particle de-agglomeration by using discrete element modelling (DEM). The DEM provides acceptable prediction of particles aerosolization when coupling with CFD (Thornton and Liu, 2004). Recently, a more sophisticate CFD-DEM model was developed. The effect of impact angle on dispersion performance was found that high angle impaction produced the higher FPF than the shallow impaction angle. Moreover, cascading impaction on two 45-degree angles improved the FPF and minimized throat deposition (Adi *et al.*, 2010). Moreover, the CFD-DEM investigation of the grid structure on the FPF generation indicated that grid plays an important role in fine powder generation (Adi *et al.*, 2010, Tong *et al.*, 2013). Whereas Coates et al. reported that the grid structure was not related to the FPF (Coates *et al.*, 2004). These results showed that frequency of impactions was one important factor in deagglomeration. However, the relation of the segregated parameters to the device geometries is still unclear and needs more investigation.

The first aim of this research was to investigate the effect of the dry powder inhalers design to the fluid dynamics characteristic and drug delivery efficiency using computational fluid dynamics. The turbulent factor and mechanical impaction fluid dynamics parameter were taken into account. The understanding in the fluid

dynamics characteristic would allow developing new dry powder inhalers. The second aim was to develop new dry powder inhalers by simple modification of commercially available devices. The computer-aid design and CFD were the basis of the development process.

OBJECTIVES

1. Study factors influencing the aerodynamics and particle dispersion in DPI device using computational fluid dynamics.

2. Evaluate dry powder inhaler devices using computational fluid dynamics.

3. Develop high performance DPI devices.

Significant Results and General discussion

Two commercially available inhalers were the Cyclohaler® and the Inhalator® (**Figure 3**). The bottom of the Cyclohaler® was capsule chamber. The Cyclohaler® had two air inlet channel (red) placed in the opposite direction in cylindrical chamber below the grid (**Figure 3A** and **3B**). A capsule would be placed in this chamber and the capsule spins inside the chamber when patients operate the device (Tong *et al.*, 2013). The upper part of the grid was the mouthpiece tube and air outlet (green). The Inhalator® has only one inlet channel (red) connected to the inlet tube at the bottom of the device. The capsule chamber was located between the grid and inlet tube. Above the grid, there was the mouthpiece that connected to bell shape outlet channel (green) (**Figure 3C** and **3D**). The narrowest channel in flow path of the Inhalator® was located at the inlet tube. The Inhalator® device internal geometries was closely related to a newer generation device, the Handihaler® (Mohammed *et al.*, 2014).

Capsules in inhaler device were pierced prior to patient's inhalation. The Cyclohaler® capsule was pierced with 2 sets of 4 small needles in the opposite direction. The needles diameter was 0.6 mm. They pierced capsule on each end of capsule cap and body, totally eight holes were created (**Figure 4A**). The Inhalator® had two needles at the same side. The needles diameter was 1.5 mm. The capsule was pierced at the side near the end of cap and body created two holes (**Figure 4B**). The air velocity in the Inhalator® was initially high at inlet channel (around 148 – 152 m/s) (**Figure 5A**). There was a different flow pattern in the capsule chamber when the capsule is present. The flow in the Inhalator® without capsule was straightforward along the inhaler length. However, with the present of capsule the high velocity inlet flow pushed the capsule toward the grid and the flow bended around the capsule (**Figure 5B**). The grid then

regulated airflow straightening the flow pattern. The velocity was gradually decreased to mouthpieces outlet channel. The flow pattern in Inhalator® mimicked a closely design, the HandiHaler® (Donovan *et al.*, 2011, Shur *et al.*, 2012).
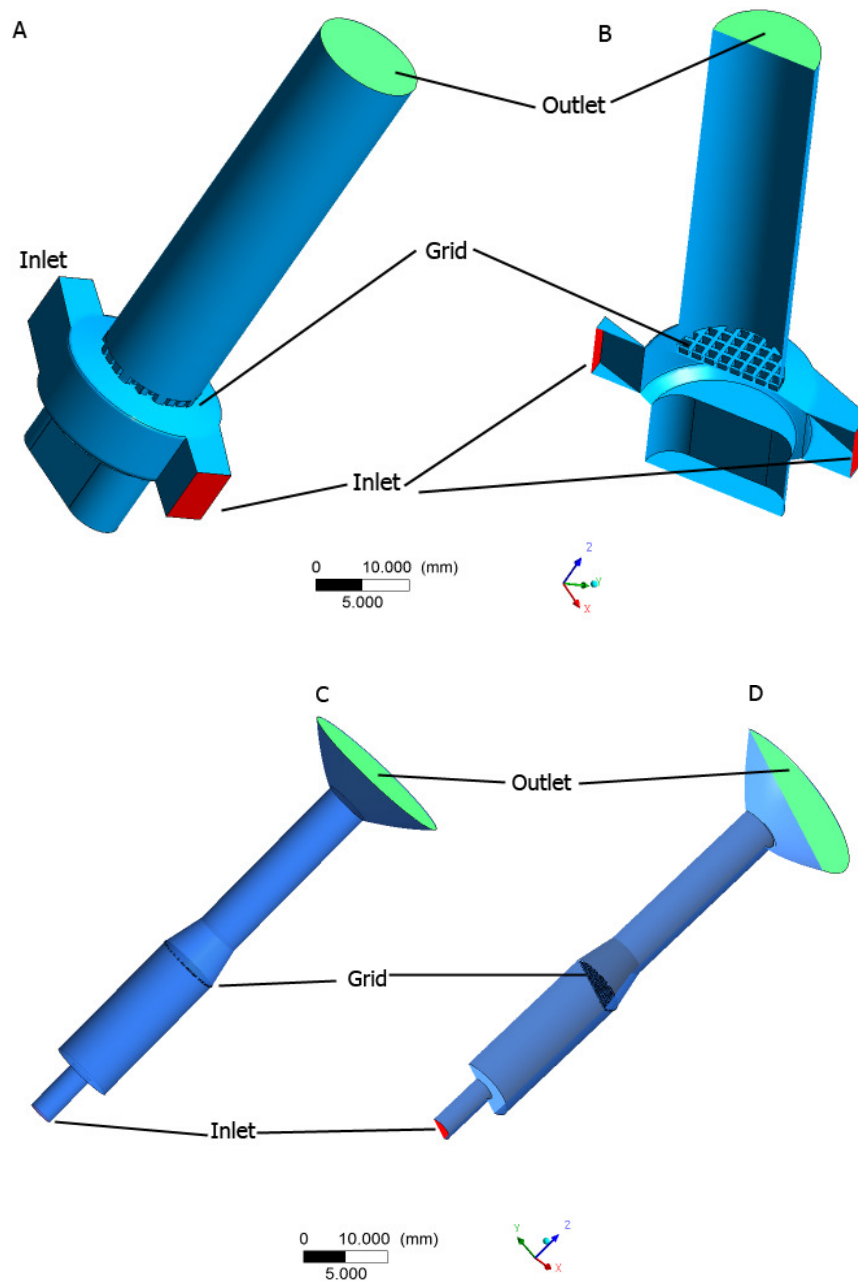
Figure 3 Internal geometries of Cyclohaler® (A and B) and Inhalator® (C and D).

The airflow pattern in the Cyclohaler® revealed that air entered the device from two inlet channels. The encounter of opposing airflow created a whirlpool-

like effects (**Figure 5C**). With the present of capsule, the swirly airflow was disrupted and changed the pattern when capsule spun around. A part of air stream drifted down the capsule to the lower chamber of the Cyclohaler®. This may change the degree for turbulence in the capsule chamber. In addition, the capsule intensified airflow velocity between the capsule and the grid. The airflow velocity at the grid part was about 19 and 20 m/s in the Cyclohaler® with and without capsule, respectively (**Figure 5C**, **5D** and **5E**). The flow pattern was similar to those of the work of Coates and coworkers (Coates *et al.*, 2004, Coates *et al.*, 2005a, Coates *et al.*, 2006, Coates *et al.*, 2007).

A   B
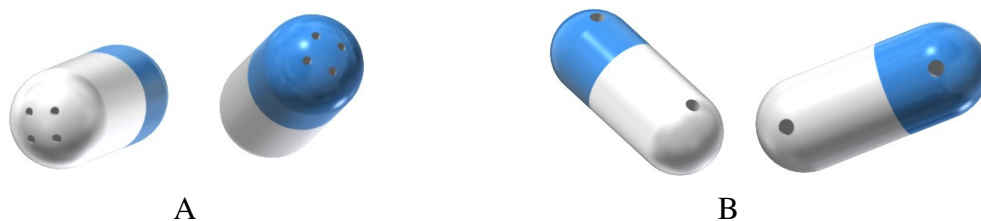
Figure 4 Pierced holes on the capsule in the Cyclohaler® and Inhalator® devices.

The Turbulent Kinetic Energy Distribution and Impaction Kinetic Energy

The turbulent kinetic energy (TKE) is a parameter that represents the fluid shear in the air-stream. The TKE in the Inhalator® was in the range of 24-550 m^2/s^2 depended on the longitudinal position of the device (**Figure 6A**). The highest TKE was located at the lower part of the device while the lowest TKE was found at the mouthpieces either the capsule inserted or removed. The highest TKE was around the middle and the bottom part of the capsule chamber in the Inhalator® without a capsule and with a capsule, respectively. The capsule largely affected the TKE around and below the grid part of the Inhalator®. The capsule obstructed the airflow path and created a localized peak TKE at the bottom part of the Inhalator® while it reduced the

TKE in other parts of the device. After the airflow passed the grid region, it did not show any variation in the TKE between the Inhalator® with and without a capsule.

The highest TKE was found in the capsule chamber of the Cyclohaler®. The Cyclohaler® without capsule showed slightly higher TKE than that the capsule was inserted. The difference in TKE was about 8%. The capsule disturbed the cyclonic airflow pattern in the capsule chamber as previously discussed. However, the capsule rotating positions do not distinctly affect the TKE level (**Figure 6B**).

The TKE in the Inhalator® was about 100 times higher than in the Cyclohaler®. Although the Inhalator® without a capsule had the lower TKE than the Inhalator® with a capsule, the TKE was still dramatically higher than in the Cyclohaler®. The small inlet tube of the Inhalator® created the high velocity of airstream that led to high turbulent magnitude.

The TKE directly controlled the impaction kinetic energy in both the Inhalator® and the Cyclohaler®. The TKE was derived from the turbulent fluctuations in a turbulent flow. The higher TKE provided more kinetic energy to particle. Thus, the impaction kinetic energy increased when the TKE had increased. In this experiment, the impaction kinetic energy was calculated in the devices without capsule. The peak impaction kinetic energy was in the capsule chamber of the Inhalator® and the Cyclohaler®. It emphasized the importance of capsule chamber design to the particles impaction processes.
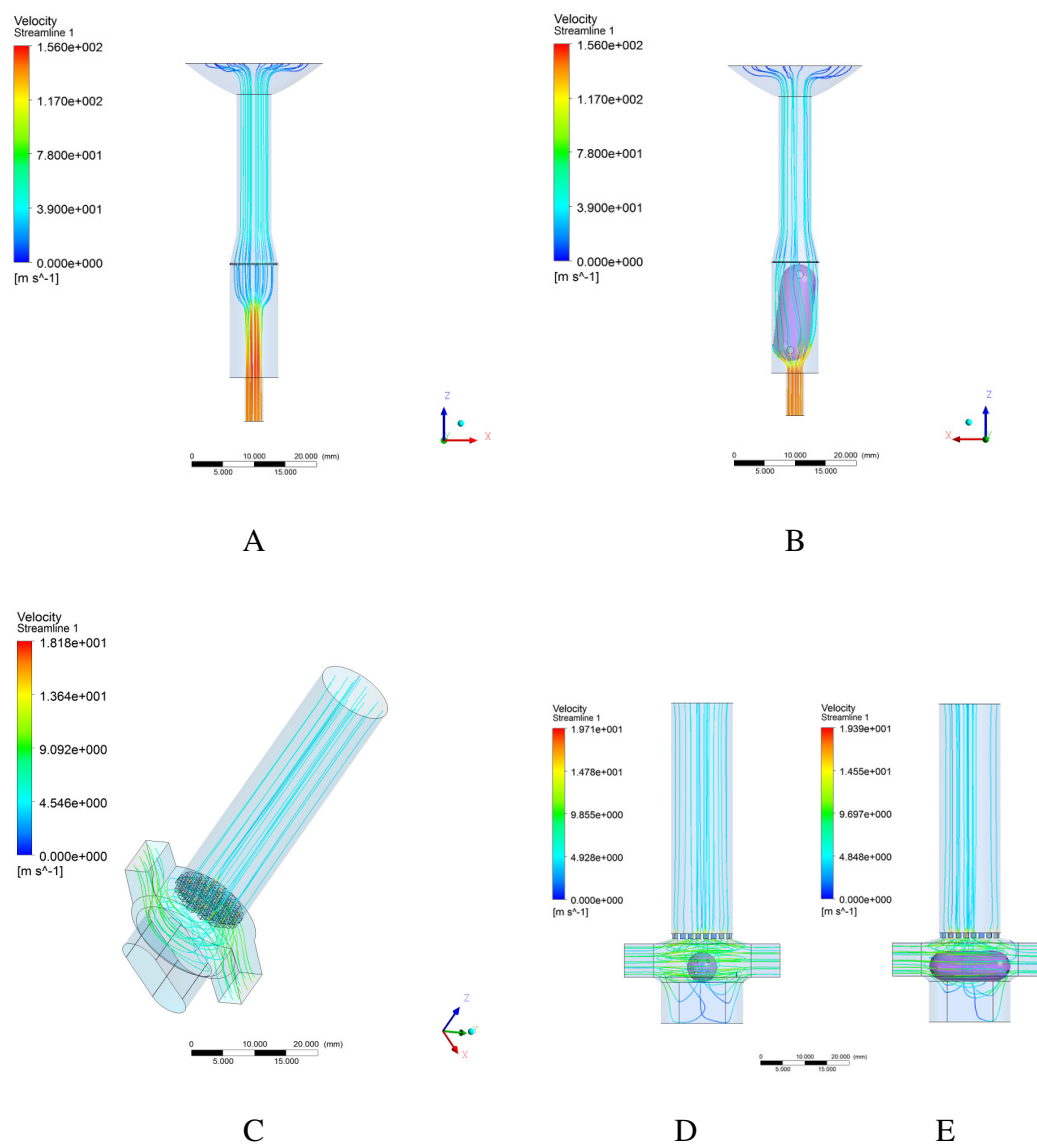
Figure 5 The velocity streamline at 60 L/min in Inhalator® device without capsule (A) or with capsule (B) and in Cyclohaler® device without capsule (C) or with capsule (D and E).

The peak impaction energy in the Inhalator® was about 2 times higher than in the Cyclohaler®, while the peak TKE of those devices was different in the magnitude of 100. It indicated that achieving high impaction kinetic energy does not require very strong TKE. In the Inhalator®, the lowest impaction kinetic energy was

located at the mouthpiece tube because the airflow was straightened and aligned with the mouthpiece. After that the impaction kinetic energy slightly increased at the mouthpiece exit due to the increment of the TKE (**Figure 6A**).
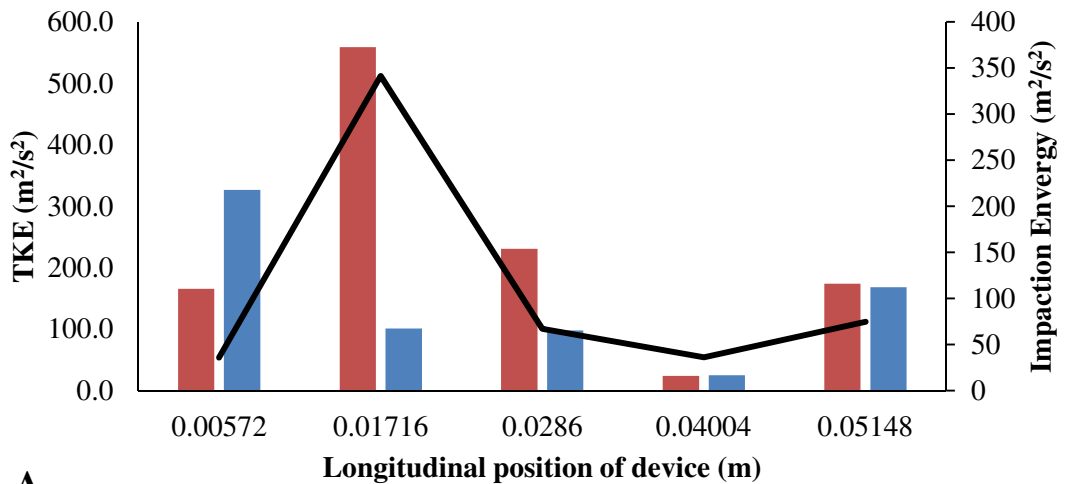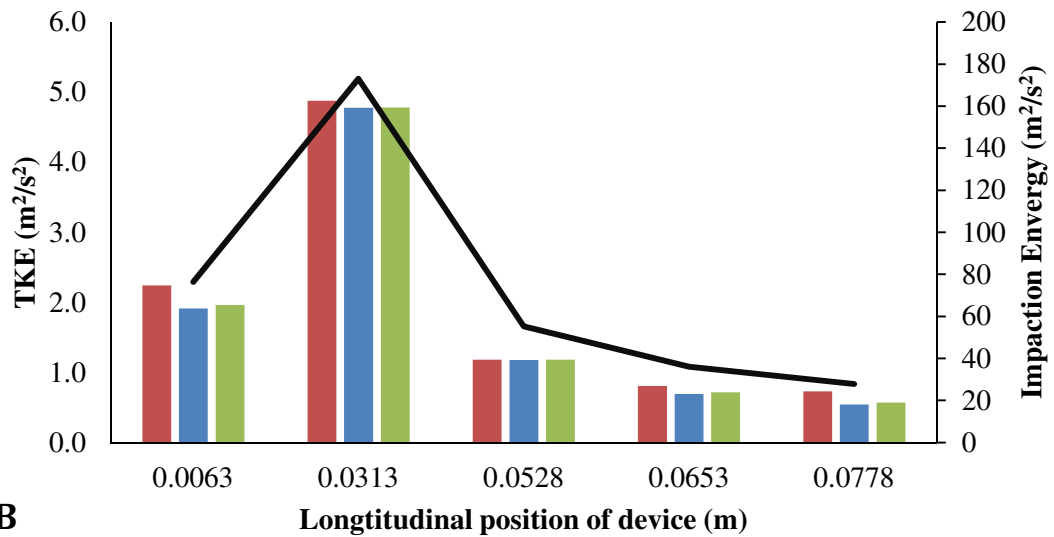
Figure 6 The TKE distribution and impaction energy (black line) in the Inhalator[®] (A) (■) without capsule, (■) with capsule and the Cyclohaler[®] (B) (■) without capsule, (■) with capsule and with capsule turned 90° (■).

The impaction kinetic energy in the Cyclohaler® was continuously decreased from the capsule chamber to the mouthpiece exit because the airflow was governed by the grid with lowering TKE (**Figure 6B**). From this result, it implied that the capsule chamber design is the most important part to improve mechanical impaction kinetic energy of the capsule based dry powder inhaler. Further dry powder inhaler designs in this research will follow the Cyclohaler® capsule chamber and the Inhalator® grid design to customize and develop new dry powder inhaler.

Computer-aided Design and Computational Fluid Dynamics Evaluation of New Dry Powder Inhaler

New dry powder inhaler designs were based on two commercially available devices, the Cyclohaler® and the Rotahaler®. The Rotahaler® was chosen as a basis design of new devices instead of the Inhalator® because the Inhalator® had too high flow resistance and required high patient's inhalation power. The cyclone-like capsule chamber was taken from the Cyclohaler®. Whereas the grid and the mouthpiece were lent from the Rotahaler®. Three dry powder inhalers were modeled using computer-aided design (CAD). The models were named as model #1, #2 and #3, respectively (**Figure 7**). The key differences in 3 models were grid position, inhaler body width and capsule insertion method. The model #1 and model #2 devices have capsule port on the side of the capsule chamber between the air inlet orifices. While the model #3 device does not have the capsule insertion port. The capsule-piercing chamber was incorporated into the bottom of model #3 device chamber. It allowed two needles to pierce the capsule from the opposite side on the tip of the capsule caps and capsule body.

The CFD Analysis and Device Performance Assessment

The flow pattern in model #1, #2 and #3 devices were swirly flow as occurred in the Cyclohaler®, especially at the capsule chamber (**Figure 8**). However there were some differences in the flow pattern. The flow pattern in model #1 device was swirly and had high velocity at the capsule chamber and the flow velocity slowed down in the inhaler body. The flow then regulated by the grid led to less swirly flow through the mouthpiece (**Figure 8A**). Whereas the flow in the capsule chamber of model #2 device had higher velocity than that occurred the model #1 and #3 devices. The narrow inhaler body of model #2 device also led to a high flow velocity. After the flow passes through the grid it also produces lower velocity flow (**Figure 8B**). The swirly flow pattern was only localized in the capsule chamber of the model #3 device because the grid was moved to the top of capsule chamber instead of near the mouthpiece outlet as in the model #1 and #2 devices.

The integral scaled strain rate (ISSR) was chosen to describe the turbulent strain on the particles. The ISSR was the ratio of turbulent dissipation to the turbulent kinetic energy (Tong *et al.*, 2013). The CFD analysis indicated that the ISSR ranged from $1592 - 3316$ s^{-1}, the probability of deagglomeration by impaction (P_{deagg}) ranged from $0.1 - 0.7$.
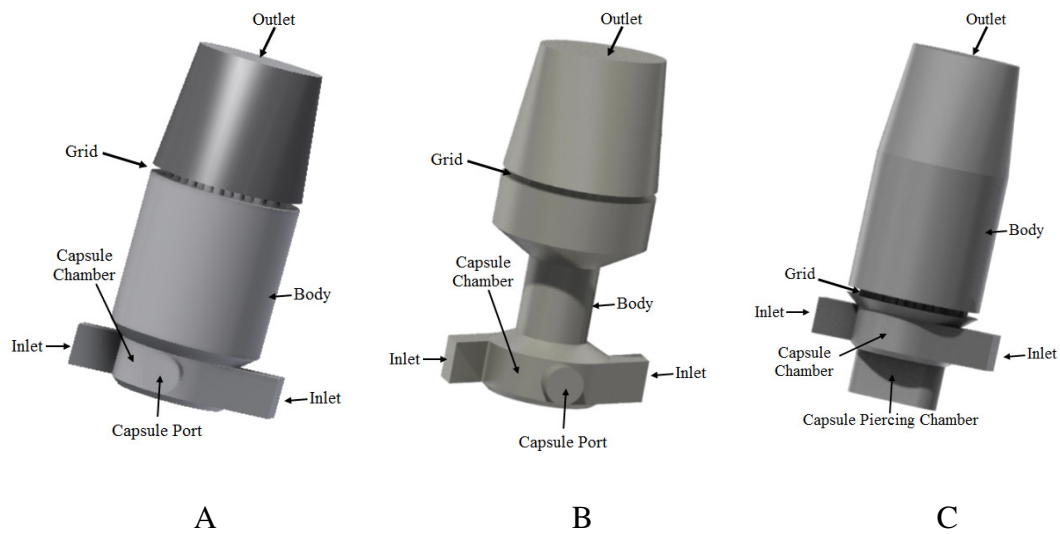
Figure 7 The internal geometries of the model #1 (A), model #2 (B)

and model #3 (C).
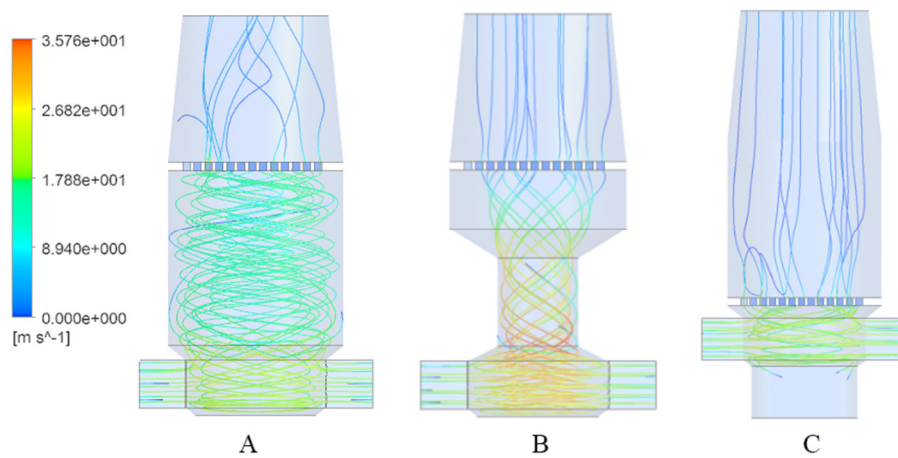
Figure 8 The flow velocity pattern in mode #1 (A), #2(B) and #3(B) at 60L/min

The ISSR could be classified into two groups 1600-2000 (the model #1 and #2 devices) and 2600-3300 (the model #2 device and the Cyclohaler®). Interestingly, the model #2 device and the Cyclohaler® had the same localized swirly flow in the capsule chamber and had higher ISSR than the model #1 and #2 devices.

Furthermore the aerosol dispersion experiment results showed that FPF was ranged from 23-50% in all devices (**Table 1**). The model #3 device generated the highest FPF (about 50%) among the 4 devices more superior than the Cyclohaler®. We found that here was no relationship between the probability of impaction deagglomeration (P_{deagg}) and the FPF. The FPF was not only affected by the P_{deagg} but also influenced by the turbulent force in the term of ISSR. The multiple linear regressions revealed that the ISSR and P_{deagg} had good relationship to the FPF with the correlation coefficient of 0.998. The statistical analysis shows the p-value of the regression parameter of 0.04 and 0.03 (**Table 2**). This supported that the ISSR and the P_{deagg} parameters were equally important parameters to predict the FPF in the Cyclohaler® derived inhaler. It confirmed the result from other research groups that the turbulent and impaction factor had important roles in deagglomeration (Coates *et al.*, 2005a, Comer *et al.*, 2001, Gac *et al.*, 2008, Selvam *et al.*, 2010). Although the ISSR and P_{deagg} had a linear correlation to the FPF, the correlation was limited to the Cyclohaler® and Rotahaler® combination design only. It may not be able to predict the behavior of other types of DPI.

Table 1 The ISSR, probability of impaction deagglomeration and FPF in Cyclohaler® device, model #1, model #2 and model #3 devices (mean ± SD, n=5)

Model	ISSR (s^{-1})	Probability of impaction deagglomeration	%FPF
Cyclohaler®	3316	0.10 ± 0.01	35.1 ± 2.3
Model #1	1592	0.39 ± 0.06	23.1 ± 2.3
Model #2	2037	0.52 ± 0.04	36.1 ± 2.8
Model #3	2565	0.69 ± 0.13	49.5 ± 1.0

The model #3 device provided well balance between the turbulence and the mechanical impaction. The frequently particle-device impaction in the model #3

was 2.5 - 17 time higher than those occurred in the Cyclohaler®, model #1 and model #2 devices. This led to a high probability of impaction deagglomeration. The grid position in the model #3 sit above the capsule chamber and was relatively similar to the Cyclohaler®. However, the grid size was larger than that in the Cyclohaler®. The swirly airflow suddenly changed the direction by the grid. It provided more particle-device impaction surface. The model #3 device could be classified as mechanical impaction dominant device.

Table 2 Multiple linear regression coefficients of the ISSR, probability of impaction deagglomeration and FPF in Cyclohaler® device, model #1, model #2 and model #3 devices.

Parameters	Coefficients	Standard Error	P-value
Constant	-15.19	2.86	0.12
ISSR	0.01	0.00	0.04
P_{deagg}	42.68	2.64	0.03

The 3D printed prototype of the model 3

The model 3 was selected as a final prototype. The model 3 prototype was separated into two parts; inhaler base and inhaler mouthpiece (**Figure 9A**). Both parts were connected together with screw thread (**Figure 9B**). The dry powder formulation capsule was pierced with 2 sets of 0.6 mm diameter needles in the opposite direction (**Figure 9B**) and put in the inhaler base as shown in **Figure 9A**.

In summary, the key methods to create efficient Cyclohaler® and Rotahaler® derived dry powder inhalers were to localize the swirly flow at the capsule chamber and intensify ISSR. Moreover, the FPF could be predicted using the

probability of impaction deagglomeration and the ISSR. The proposed model 3 is reasonable for further development of dry powder inhalers.

Figure 9 The 3D printed prototype of model 3 (A and B) and pierced capsule (C).

CONCLUSIONS

The aerodynamic processes in the dry powder inhalers were investigated in this study. The loose agglomerated dry powder formulations were aerosolized by two major mechanisms; the aerodynamic turbulent shear dispersion and the mechanical impaction deagglomeration. The aerodynamic turbulent shear forces can be expressed by two parameters that were the TKE and the ISSR. We found that the TKE had highly correlated with the impaction energy and the probability of deagglomeration by impaction. The FPF and the TKE also had well correlation. Moreover the small carrier size sharply responded to the TKE when compared to large lactose carrier formulation. Slightly elevation of the TKE led to largely increase the FPF in the small carrier size formulation. We also observed that the strategies to increase the TKE were by adding a swirly flow as in the Cyclohaler® and using the narrow flow-path as in the Inhalator®. The whirlpool-like swirly flow in the Cyclohaler® was a result of a cyclonic chamber that created a tangential flow across the axial flow. Furthermore, a swirly flow also increased the particle-device impactions. On the other hand, the Inhalator® had different mechanism. It had a straight tube design with a grid. The grid rapidly changed the airflow directions and elevated the turbulence. In addition the grid also provided impaction surface for the agglomerated particles. The narrow airflow path in the Inhalator® maximized the air velocity and created the energetic particle-device impaction and the intense shear force. Nevertheless, the high velocity particle had a drawback that it increased the inertial impaction on the upper airways and would cause some loss of the drug. The cyclone chamber design of the Cyclohaler® and the grid design of the Inhalator® were the basis of the proposed inhaler devices. The CAD and CFD design pipeline was proven their potential for use as higher performance inhaler

devices. The model 3 device had the best performance in both the CFD simulation and the experimental result. It can generate 50% FPF and had a low MMAD when operated at 60 LPM with the Ventolin Rotacaps®. Moreover, the inhaler that was derived from the Cyclohaler® design was highly dependent on the grid position. Placing the grid adjacent to the swirly airflow chamber did improve the aerosolization performance.

Recommendation and Limitation

Recommendation and limitation of this thesis are stated below.

1. The grid in the capsule based DPI should have minimal effects on pressure drop to ensure the performance of the device in the patients. The grid should retain its ability to prevent capsule fragments entering the airways and straighten the airflow in the mouthpiece. The grid size should not create overall pressure drop across device over 10 mbar$^{1/2}$/LPM to ensure a comfortable operation of the patients (Clark and Hollingworth, 1993).

2. For practical use of the model #3 device, the screw connection between the chamber and the mouthpiece of the model #3 device should be modified. A snap locking mechanism may replace the screw connection for convenience. In addition, a simpler capsule piercing mechanism has to be developed.

3. The CFD simulation in this research was performed without capsule due to limitation of the computaional power. However, there were several evidences from previous works that the capsule had a minimimal effect on the aerosolization process (Coates *et al.*, 2005b).

4. The airflow velocity directly affected the FPF. Increment of airflow velocity creates more drag force on the particles (Equation 1). The particle-device impaction

increases with a high particle velocity resulting in a better drug deagglomeration

and FPF.

$$F_d = \frac{1}{2}\rho v^2 C_d A \qquad\qquad \text{Equation 1}$$

ρ is the particle density,
v is the speed of the object relative to the fluid
C_d is the drag coefficient,
A is the cross section area

REFERENCES

Adi, H., Kwok, P. C., Crapper, J., Young, P. M., Traini, D. & Chan, H. K. 2010. Does electrostatic charge affect powder aerosolisation? *J Pharm Sci,* 99**,** 2455-61.

Anthony, T. R. e. & Flynn, M. R. 2006. Computational fluid dynamics investigation of particle inhalability. *J Aerosol Sci,* 37**,** 750-765.

AstraZeneca 2010. Pulmicort Flexhaler® prescribing in formation. Södertälje, Sweden: AztraZeneca AB.

Ball, C. G., Uddin, M. & Pollard, A. 2008. High resolution turbulence modelling of airflow in an idealised human extra-thoracic airway. *Comput Fluids,* 37**,** 943–964.

Cheng, Y. S. 2014. Mechanisms of pharmaceutical aerosol deposition in the respiratory tract. *AAPS PharmSci,* 15(3), 630-40.

Clark, A. R. & Hollingworth, A. M. 1993. The relationship between powder inhaler resistance and peak inspiratory conditions in healthy volunteers — implications for *in vitro* testing *J Aerosol Med,* 6**,** 99-110.

Coates, M. S., Chan, H.-K., Fletcher, D. F. & Raper, J. A. 2005a. Influence of air flow on the performance of a dry powder inhaler using computational and experimental analyses. *Pharm Res,* 22**,** 1445-1453.

Coates, M. S., Chan, H. K., Fletcher, D. F. & Chiou, H. 2007. Influence of mouthpiece geometry on the aerosol delivery performance of a dry powder inhaler. *Pharm Res,* 24**,** 1450-1456.

Coates, M. S., Chan, H. K., Fletcher, D. F. & Raper, J. A. 2006. Effect of design on the performance of a dry powder inhaler using computational fluid dynamics. Part 2: Air inlet size. *J Pharm Sci,* 95**,** 1382-1392.

Coates, M. S., Fletcher, D. F., Chan, H.-K. & Raper, J. A. 2005b. The role of capsule on the performance of a dry powder inhaler using computational and experimental analyses. *Pharm Res,* 22**,** 923-932.

Coates, M. S., Fletcher, D. F., Chan, H. K. & Raper, J. A. 2004. Effect of design on the performance of a dry powder inhaler using computational fluid dynamics. Part 1: Grid structure and mouthpiece length. *J Pharm Sci,* 93**,** 2863-2876.

Comer, J. K., Kleinstreuer, C. & Zhang, Z. 2001. Flow structures and particle deposition patterns in double-bifurcation airway models. Part 1. Air flow fields. *J Fluid Mech,* 435**,** 25-54.

Daniher, D. I. & Zhu, J. 2008. Dry powder platform for pulmonary drug delivery. *Particuology,* 6**,** 225-238.

Depreter, F., Pilcer, G. & Amighi, K. 2013. Inhaled proteins: Challenges and perspectives. *Int J Pharm,* 447**,** 251-280.

Donovan, M. J., Kim, S. H., Raman, V. & Smyth, H. D. 2011. Dry powder inhaler device influence on carrier particle performance. *J Pharm Sci,* 101**,** 1-11.

El-Gendy, N., Huang, S., Selvam, P., Soni, P. & Berkland, C. 2012. Development of budesonide nanocluster dry powder aerosols: Formulation and stability. *J Pharm Sci,* 101**,** 3445-3455.

Gac, J., Sosnowski, T. R. & Gradon, L. 2008. Turbulent flow energy for aerosolization of powder particles. *J Aerosol Sci,* 39**,** 113-126.

Grant, M. & Leone-Bay, A. 2012. Peptide therapeutics: it's all in the delivery. *Ther Deliv,* 3**,** 981-996.

Hoppentocht, M., Hagedoorn, P., Frijlink, H. W. & de Boer, A. H. 2014. Technological and practical challenges of dry powder inhalers and formulations. *Adv Drug Deliv Rev,* In Press.

Islam, N. & Cleary, M. J. 2012. Developing an efficient and reliable dry powder inhaler for pulmonary drug delivery – A review for multidisciplinary researchers. *Med Eng Phys,* 34**,** 409-427.

Islam, N. & Gladki, E. 2008. Dry powder inhalers (DPIs) - A review of device reliability and innovation. *Int J Pharm,* 360**,** 1-11.

Kandasam, R. & Chandrasekaran, K. 2013. Sustained release aerosol for pulmonary drug delivery system: A review. *Int J Pharm Pharm Sci,* 5**,** 126-130.

Karner, S., Maier, M., Littringer, E. & Urbanetz, N. A. 2014. Surface roughness effects on the tribo-charging and mixing homogeneity of adhesive mixtures used in dry powder inhalers. *Powder Technol,* 264**,** 544-549.

Kleinstreuer, C. & Zhang, Z. 2003. Laminar-to-turbulent fluid-particle flows in a human airway model. *Int J Multiphas Flow,* 29**,** 271-289.

Kleinstreuer, C., Zhang, Z., Li, Z., Roberts, W. L. & Rojas, C. 2008. A new methodology for targeting drug-aerosols in the human respiratory system. *Int J Heat Mass Tran,* 51**,** 5578-5589.

Lee, S., Adams, W., Li, B., Conner, D., Chowdhury, B. & Yu, L. 2009. In vitro considerations to support bioequivalence of locally acting drugs in dry powder inhalers for lung diseases. *AAPS Pharmsci,* 11**,** 414-423.

Longest, P. W., Son, Y. J., Holbrook, L. & Hindle, M. 2013. Aerodynamic factors responsible for the deaggregation of carrier-free drug powders to form micrometer and submicrometer aerosols. *Pharm Res.,* 30**,** 1608-27.

Milenkovic, J., Alexopoulos, A. H. & Kiparissides, C. 2013. Flow and particle deposition in the Turbuhaler: A CFD simulation. *Int J Pharm,* 446**,** 205-213.

Mohammed, H., Arp, J., Chambers, F., Copley, M., Glaab, V., Hammond, M., Solomon, D., Bradford, K., Russell, T., Sizer, Y., Nichols, S., Roberts, D., Shelton, C., Greguletz, R. & Mitchell, J. 2014. Investigation of dry powder inhaler (dpi) resistance and aerosol dispersion timing on emitted aerosol aerodynamic particle sizing by multistage cascade impactor when sampled volume is reduced from compendial value of 4 L. *AAPS PharmSciTech,* 15(5), 1126-37.

Ramsey, J. M., Hibbitts, A., Barlow, J., Kelly, C., Sivadas, N. & Cryan, S.-A. 2013. 'Smart' non-viral delivery systems for targeted delivery of RNAi to the lungs. *Ther Deliv,* 4**,** 59-76.

Selvam, P., McNair, D., Truman, R. & Smyth, H. D. C. 2010. A novel dry powder inhaler: Effect of device design on dispersion performance. *Int J Pharm,* 401**,** 1-6.

Shur, J., Lee, S., Adams, W., Lionberger, R., Tibbatts, J. & Price, R. 2012. Effect of device design on the in vitro performance and comparability for capsule-based dry powder inhalers. *AAPS J,* 14**,** 667-676.

Srichana, T., Martin, G. P. & Marriott, C. 1998. On the relationship between drug and carrier deposition from dry powder inhalers in vitro. *Int J Pharm,* 167**,** 13-23.

Thornton, C. & Liu, L. 2004. How do agglomerates break. *Powder Technol,* 143–144**,** 110–116.

Timsina, M. P., Martin, G. P., Marriott, C., Ganderton, D. & Yianneskis, M. 1994. Drug delivery to the respiratory tract using dry powder inhalers. *Int J Pharm,* 101**,** 1-13.

Tong, Z., Zheng, B., Yang, R., Yu, A. & Chan, H. 2013. CFD-DEM investigation of the dispersion mechanisms in commercial dry powder inhalers. *Powder Technol,* 240**,** 19–24.

Voss, A. & Finlay, W. H. 2002. Deagglomeration of dry powder pharmaceutical aerosols. *Int J Pharm,* 248**,** 39-50.

Wong, W., Fletcher, D. F., Traini, D., Chan, H.-K., Crapper, J. & Young, P. M. 2010. Particle aerosolisation and break-up in dry powder inhalers 1: evaluation and modelling of venturi effects for agglomerated systems. *Pharm Res,* 27**,** 1367-1376.

Yang, M. Y., Chan, J. G. Y. & Chan, H.-K. 2014. Pulmonary drug delivery by powder aerosols. *J Control Release,* 193, 228–240.

Zhang, Y., Finlay, W. H. & Matida, E. A. 2004. Particle deposition measurements and numerical simulation in a highly idealized mouth-throat. *J Aerosol Sci,* 35**,** 789-803.

Zhou, Q. T., Tang, P., Leung, S. S. Y., Chan, J. G. Y. & Chan, H.-K. 2014. Emerging inhalation aerosol devices and strategies: Where are we headed? *Adv Drug Deliv Rev,* 75, 3–17.

Zhou, Y. & Cheng, Y. S. 2000. Particle deposition in first three generations of a human lung cast. *J Aerosol Sci,* 31**,** 140-141.

APPENDICES

Appendix 1   Reprint of papers and manuscripts

Appendix 2   Vitae

Reprint of papers and manuscripts

PAPER 1

Effect of turbulent kinetic energy on dry powder inhaler performance

(Published in *Powder Technology*)

Contents lists available at ScienceDirect

Powder Technology

Effect of turbulent kinetic energy on dry powder inhaler performance

Tan Suwandecha [a], Wibul Wongpoowarak [a], Kittinan Maliwan [b], Teerapol Srichana [a,c,*]

[a] Department of Pharmaceutical Technology, Faculty of Pharmaceutical Sciences, Prince of Songkla University, Songkhla, Thailand
[b] Department of Mechanical Engineering, Faculty of Engineering, Prince of Songkla University, Hat Yai, Songkhla, Thailand
[c] Drug Delivery System Excellent Center, Faculty of Pharmaceutical Sciences, Prince of Songkla University, Songkhla, Thailand

ARTICLE INFO

ABSTRACT

Dry powder inhalers (DPIs) have been extensively used for delivering medication to the lungs. Different designs of DPI devices affect the aerosolization processes of the drug particles. The processes cannot be easily visualized in experiments, thus computational fluid dynamics were used to investigate the turbulence kinetic energy and particle impaction. In this research, 3 size ranges of lactose carrier and the Cyclohaler® and Inhalator® devices were used as models for the computational simulations. The velocity vector, the turbulence kinetic energy (TKE) and particle trajectory were obtained. An aerosol dispersion experiment was performed using the Andersen Cascade Impactor. The TKE was directly related to the flow-rate. The TKE in the Cyclohaler® was lower than that in the Inhalator® due to its narrow geometry and this resulted in a high velocity air-flow. In the Cyclohaler® the probability of deagglomeration by impaction was high because of the cyclone-like design while the cross grid of the Inhalator® was an important factor for deagglomeration of the particles. The FPF varied from 7 to 30% and the FPF increased as the flow-rate increased. The MMAD was in the range of 4–6 μm. The carrier size also affected the probability of deagglomeration at 60 and 90 L/min, but not at 30 L/min. In summary, maximizing the TKE and the particle impaction rate by adding a grid and providing a cyclone-like design was key factor to achieve a high deagglomeration of the particles.

© 2014 Elsevier B.V. All rights reserved.

1. Introduction

Dry powder inhalers (DPIs) have been extensively used for delivering medication to the lungs. This is a good choice, especially for delivering bronchodilator and corticosteroids to asthmatic patients [1]. Many research works have extended DPI applications for systemic drug delivery such as for insulin. Currently available DPI devices have various designs such as for their mouthpieces, air inlet channels and the aerosolization chambers each leading to differences in the aerodynamic characteristics [2–4] of the air flows. The different designs of the device greatly affect the DPI performance such as the Fine Particle Fraction (FPF) and the Mass Median Aerodynamic Diameter (MMAD) [5].

1.1. DPI formulations

The formulation of DPIs usually employs lactose as a bulk carrier with only a few milligrams of the drug. The drug to carrier ratios can be varied such as 1:67.5 (Diskhaler®, Rotahaler® and Cyclohaler®), 1:4.6 (Pulmicort Flexhaler 180 μg®) and 1:24 (Inhalator®) [6,7]. The mixing of lactose and drug particles also improves the efficiency of drug delivery by reducing drug particle aggregations [1]. After aerosolization process in a DPI device, the large carrier particles deposit on the

upper airways, whereas the smaller drug particles reach the lower parts of the lungs [8].

1.2. Interparticulate force and aerodynamic force

Drug particles loosely attach to the surface of the lactose carrier with inter-particle force such as Van der Waals force, capillary force and electrostatic force. The Van der Waals force is a molecular attraction and repulsive interaction on the surface of particles. For ideal system with smooth spherical particles, Van der Waals force is a function of particle radius and separation distance. The Van der Waals separation radius of particles is affected by the surface roughness and shape of particles that controlled the contact areas between particles. High surface roughness reduces the contact area (increases separation distance) while a flat surface of particles increases the contact area (decreases separation distance). The surface asperities having effective separation distances above 1 μm remove the Van der Waals force [9]. The Van der Waals force becomes more significant as the particle size decreases [10]. The Van der Waals attraction dominates in particles of less than 20 μm as the pick-up of velocity from the powder bed was significantly increased, while the 40–100 μm particle pick up of velocity was not much different [11]. In this manner, micrometer domain particles were not significantly affected by the Van der Waals forces [12]. The capillary force and electrostatic force are briefly two times weaker than the Van der Waals in a moderate humidity [10]. However, if the humidity increases the

* Corresponding author.
  E-mail address: teerapol.s@psu.ac.th (T. Srichana).

capillary force will become dominant and as electrostatic forces weaken the Van der Waals force becomes insignificant [13]. The carrier particle in the DPI formulation is usually in the range of 50–100 μm so that the fluid force in the DPI device is strong enough to overcome the adhesion force [1,14].

During the aerosolization process, the drug particles are detached from the carrier surface if the energy from either the fluid shear or mechanical impaction overcomes the adhesion forces between the drug-carrier particles [15,16]. The viscous force acting on particles is a drag force (F_{drag}) that is related to particle cross-sectional area (d^2) (Eq. (1)). For particle collision the inertial force is the kinetic energy function (E_k) that is proportional to the particle volume (d^3) (Eq. (2)).

$$F_{drag} = C_d \frac{\pi}{8} \rho_a d^2 V^2 \tag{1}$$

$$E_k = \frac{\pi}{12} \rho_p d^3 V^2 \tag{2}$$

C_d drag coefficient
d diameter of the particles (m)
V fluid velocity (m/s)
ρ_p, ρ_a Particle density, fluid density (kg/m3), respectively.

1.3. The computational assisted DPI research

Computational fluid dynamics (CFD) is used in engineering fields and is now also gaining in popularity in some areas of pharmaceutical research [3,17–19]. It is useful for investigating aerodynamic parameters such as the turbulence kinetic energy (TKE), pressure and aerodynamic shear force and the trajectory of particles. These parameters allow us to better understand the aerosolization processes in the DPI devices than any in vitro experiments. There was an attempt to use the non-dimensional specific dissipation (NDSD) parameter to predict dispersion performance in carrier-free DPI devices. The NDSD was classified into 3 categories, flow-based factor, turbulence based factor and particle based factor. The flow-based factor such as pressure drop and flow-rate had a weak correlation to dispersion performance. The turbulence-based factors such as TKE and turbulence intensity (TI) and particle-based factors such as wall impaction count and average trajectory integral were fairly to weakly predict MMAD [20]. However, some research indicated that particle–wall impaction dominated in powder dispersion mechanism [21]. The level of turbulence and particle collisions is influenced by the air inlet channel while the design of the mouthpiece controls the outlet air velocity and flow pattern [22]. The flow pattern in the device and the outlet air velocity may cause drug loss in the oropharyngeal region by inertial impactions [23]. In addition to the experimental approach of Voss and Finley, they found that turbulence was also an important mechanism by adjusting the magnitude of the turbulence thus maximizing the particle impaction velocity. Whereas, the effect of the mechanical impaction on the dispersion of the particles was still unclear in the salbutamol sulfate–lactose carrier DPI dispersion [24]. Recently, discrete element modeling (DEM) was used to dynamically simulate particle de-agglomeration. It provided acceptable prediction of particle aerosolization when coupled with CFD [25]. The CFD–DEM coupling could analyze the interaction collision between particles–particles and particle–wall. The investigation in the Aerolizer® device indicated that the particle–wall impaction had a major role in deagglomeration especially in the dispersion chamber of the inhaler [26]. Although the DEM method offers a sophisticated computational analysis, this method needs high computational power and the coupling scheme is still limited to small numbers of large particles [27].

In this research, the carrier particle–wall impaction using only the CFD discrete particle model without DEM would be simpler and less computational intensive than that of the CFD–DEM. The aims of this research were to investigate the TKE, particle impaction and device performances for delivery of the drug during the aerosolization processes in the DPI devices using simple CFD particle tracking.

2. Materials and methods

2.1. Preparation of the lactose carrier

The particle size of the lactose carrier in the range of 10–100 μm was prepared by the use of a Ball mill (Planetary MonoMill pulverisette 6, Fritsch GmbH, Idar-Oberstein, Germany) operating at 350 rpm for 1 h. Milled carrier particles were separated by size with a sieve series having open diameters of 90, 71, 30 and 20 μm. The separated size ranges of the carrier in this study were from 71–90, 30–71 and 20–30 μm. These three size fractions of lactose carrier were used to prepare formulations #1, #2 and #3 respectively to investigate their different drug delivery efficiencies.

2.2. Particle size distribution measurement and fitting

Carrier sizes were determined using a laser diffraction technique (Beckman Coulter LS 230, CA, USA). In this study, the dispersion medium was prepared by suspending lactose in methanol overnight and the lactose saturated methanol was filtered through a 0.22 μm membrane. Lactose particles were suspended in a dispersion medium. Ultrasonication was used for 15 s to reduce lactose particle aggregation (Ultrasonicator, Elma, Germany). A background measurement was taken first and then the sample was added and mixed homogeneously with the medium until the percentage obscuration was about 10. The particle size distribution was calculated as the volume median diameter and its associated geometric standard deviation. Five measurements were carried out for each sample. The particle size distribution was fitted to the Rosin–Rammler equation to obtain the distribution parameter for the computational simulation (Eq. (3)). The fitting was solved using the Microsoft Excel® GRG nonlinear solver optimizing k and λ for minimal root mean square error between fitted and raw data.

$$F(x, k, \lambda) = \begin{cases} 1 - e^{-(x-\lambda)^k} & , x \geq 0 \\ 0 & , x < 0 \end{cases} \tag{3}$$

$F(x; k; \lambda)$ is the fraction of particles with diameter <x.
λ is the mean particle size.
k is a particle size spread.

2.3. Formulation of the salbutamol dry powder inhaler

The formulations were prepared by mixing micronized salbutamol sulfate (DDSA Pharmaceutical, London, UK) with lactose carrier at a ratio of 1:67.5 w/w. Each formulation contained 40 mg of drug and 2.7 g of each carrier in a vial. Hand mixing was carried out for 10 min, and then mixed using a Turbula® mixer for 30 min (Willy A. Bachofen AG Maschinenfabrik, Switzerland). The uniformity of powder blends in each formulation was determined by five random samplings from different positions of the formulation powder for an assay of salbutamol sulfate content. The sampled powder was dissolved with water, diluted to an appropriate concentration and analyzed using a spectrofluoroscopic technique with an excitation wavelength of 218 nm and an emission wavelength of 309 nm [28]. The powder mix was filled into no. 3 capsules (1 dose = 27.4 mg, consisting of 400 μg drug), for use with two commercial inhaler devices (Cyclohaler® Pharbita, Netherlands and Inhalator® Boerhinger Ingelheim, Germany).

2.4. Drug deposition studies

The drug deposition was evaluated using the 8-stage Andersen Cascade Impactor (ACI; Copley Scientific Limited, Nottingham, UK),

34

which was operated at 30, 60 and 90 L/min for 20, 10 and 6.7 s, respectively. The operating relative humidity was controlled at 50 ± 5%. The ACI stages were varied depending upon the flow-rate, and in these experiments we used stages 0 to 7, −1 to 6 and −2 to 5 for a flow-rate of 30, 60 and 90 L/min, respectively. The amount of drug deposited on each collection plate in each stage was eluted with water to obtain its concentration. Quantitative analysis was carried out by a fluorescence technique [28]. The percent deposition was calculated on each stage. The percentage Fine Particle Fraction (%FPF) and the Mass Median Aerodynamic Diameter (MMAD) were used to determine the performance of the drug delivery. The percent Emission (%EM) was calculated from the percentage of the drug emitted from the device. %FPF was calculated from a summation of the amount of drug retained on the stage at a cut-off diameter of below 5 μm.

2.5. Computational simulation

The dimensions of the Cyclohaler® and Inhalator® devices were precisely measured using a Vernier caliper. A 3D model of the DPI devices was created using Gambit® software (ANSYS, Inc., USA). The 3D models were meshed to create computational nodes. The mesh quality was controlled using the equiskewness parameter that determined the deviation of the mesh shape from the hexagonal to the tetrahedral shape. CFD problems were solved using the finite volume method of the Fluent® software package (ANSYS, Inc., USA). The solving of the fluid dynamic was based on the momentum, mass and energy conservation (Navier–Stoke equation). The turbulence model was the k–ε where k and ε describe the turbulence kinetic energy and turbulent dissipation rate, respectively. The second-order upwind schemes were applied to discretize the partial differential equations of a momentum, TKE and turbulent dissipation rate. A semi-implicit method for pressure linked equation (SIMPLE) algorithm was used for the coupling of the mass and momentum equations [29]. The CFD iteration was repeated until the residual error was less than 1×10^{-3}. Simulation condition was set as standard ambient temperature and pressure (SATP) condition. The boundary conditions used for an inhaler outlet equal to a velocity inlet (volume flow-rate was converted to the velocity flow-rate) and a 0 bar relative pressure of an inhaler inlet. For simulation of the dispersion of the particles, only carrier particles were simulated because the mass of the drug particles was very small when compared to that of the carrier particles. Therefore, the dispersion efficiency was controlled mainly by the properties of the carrier [30]. Post-processing of the CFD simulation was analyzed for the following properties.

2.5.1. Velocity contour and turbulence kinetic energy (TKE)
The velocity contour and turbulence kinetic energy were plotted to visualize the flow characteristics in the inhaler devices.

Table 1
Discrete phase model parameters.

DPM parameters	
Max tracking step	500,000
Drag law	Spherical
Stochastic tracking	5 tries with discrete random walk
Injected particles	200
Particle size distribution	Rosin–Rammler
Injection type	Group

2.5.2. Particle trajectory and particle interactions
The assumptions made for the tracking of particles were no particle–particle interactions and no particle breakups. The particle–particle interaction was negligible because the carrier particle occupied a fairly low volume fraction [31]. This was due to the fact that the ratio of the particle mass to the total system volume was very low (dilute system). Therefore, we considered only the particle–wall interaction and focused on the impaction of the lactose carrier on the wall of the devices. A discrete phase model (DPM) was used to simulate the particle trajectory. The particles were injected from the points where powder aerosolization occurred in either the Cyclohaler® or the Inhalator®. The DPM parameters are described in Table 1. The maximum tracking step is 500,000 so it was a large population enough to ensure that all particles could escape from the system. In this simulation we assumed that all particles were spherical in shape. A group of 200 particles was injected into the system and 5 tries of stochastic tracking were used to mimic real randomness in the particle trajectory. The particle size distribution was by a Rosin–Rammler or Weibull distribution. The outlet of each device was set as an escape boundary for particle tracking. The particle–wall impaction was assumed as fully bounced by using the restitution coefficient of 1 [20].

The particle–wall impaction data were obtained from the particle impaction counts. The impaction velocity was collected and converted to the probability of an agglomerated particle breakup. The particle–wall impaction count described the frequency of the impaction. In a similar manner, the impaction velocity estimated the kinetic energy of impaction which was calculated to the kinetic energy per unit mass. The kinetic energy of impaction was calculated using the velocity (u, v and w) in three axes (x, y and z axes) (Eq. (4)).

$$K_e/m = u^2 + v^2 + w^2 \tag{4}$$

where K_e/m is the kinetic energy per unit mass, and u, v and w are the particle velocities in the x, y and z axis, respectively. In this study, the drug-carrier particle agglomerate was assumed as a single large particle equivalence and because mass of carrier was much larger than drug carrier that adhered on, only carrier particle can be used for simulation.
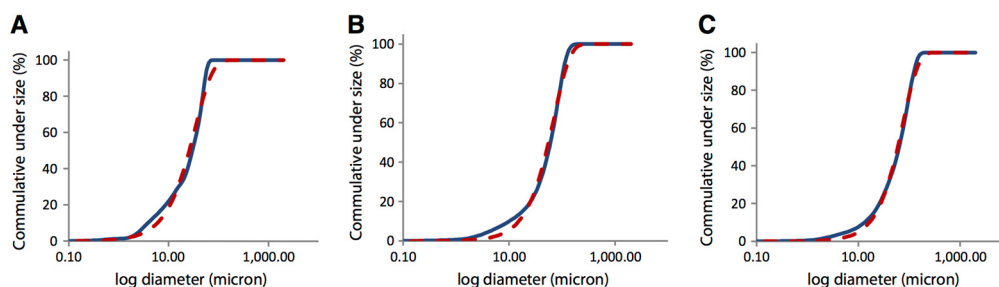
Fig. 1. Commulative log-under size plot of fine (A), medium (B) and coarse (C) lactose carriers. Solid line is the raw data and dash line is the fitting curve.

Table 2
Lactose carrier particle size distribution.

Sample	Sieve size	Mean (µm)	Span
Lactose fine	20–30 µm	33.0	1.27
Lactose medium	30–71 µm	68.0	1.46
Lactose coarse	71–90 µm	72.9	1.47

Upon impaction, the impaction energy creates stress on particles and drug detachment from carrier particles like particle breakup. The probability of an agglomerated particle breakup by impaction depended on the frequency of the impaction, the impaction energy, particle sizes, threshold energy of break-up and a break-up resistance of the parameter for each material (Eq. (5)) [32].

$$P = 1 - e^{-f_{mat} dk (W_m - W_{m,min})} \qquad (5)$$

$W_{m,min}$	threshold energy of break-up
W_m	impact energy
d	particle diameter
f_{mat}	break-up resistance parameter
k	impact frequency.

Since the material parameters $W_{m,min}$ and f_{mat} in this simulation are constant, Eq. (4) is simplified by neglecting the threshold energy of break-up and the break-up resistance parameters (Eq. (6)).

$$P = 1 - e^{-dkW_m} \qquad (6)$$

Electrostatic charges occur during the aerosolization process from a triboelectric effect. The triboelectric effect is caused by two different materials contacting together through friction and surface charge transfer from one material surface to another material surface. During the aerosolization process electrostatic charges had a linear increment with aerosolization air flow [13]. Measurement of the electrostatic charges during aerosolization was conducted using a Faraday's pail and a NanoCoulomb electrometer Model 284 (Monroe Electronics Inc., NY, USA). An inhaler device with dry powder formulation was placed in the center of the Faraday's pail and connected to a vacuum pump.

3. Results and discussion

3.1. Lactose carrier particle size distribution

The Rosin–Rammler fitting shows that the span of particle sizes was around 1.2–1.5 µm (Fig. 1). The mean particle sizes of the fine, medium and coarse lactose carrier were 33.0, 68.0 and 72.9 µm, respectively

(Table 2) [33]. The span of the carrier particle size was larger than 1. This means that the size distribution is not monodisperse.

3.2. Drug deposition studies

Salbutamol sulfate and lactose formulations showed good uniformity. The FPF varied from 7 to 30% and the overall trend increased with flow-rate. The FPF of the Cyclohaler® device (Fig. 2A) was quite low at a flow rate of 30 L/min (7–15%). At a flow-rate of 60 L/min, the FPF sharply increased when compared to the 30 L/min whereas at 90 L/min FPF was slightly higher than 60 L/min. The carrier size has an effect on the FPF in some conditions. The medium sized lactose carrier had the highest FPF at all flow-rates. The small and large lactose carriers did not have much difference in their FPF values. This result indicated that the Cyclohaler® operated well at flow rates of over 60 L/min and the formulation with the medium sized lactose carrier had the best performance.

The Inhalator® device at 30 L/min had a low FPF (7–16%) (Fig. 2B). The formulation with the small size lactose carrier had the smallest FPF while there was little difference between the medium and large carriers. At a flow-rate of 60 L/min the FPF of the formulation with the medium sized lactose carrier had a slightly higher FPF than with the small and large carriers and overall the FPF was also higher than for the 30 L/min. The FPF at 90 L/min with the formulation of small and large size carriers was slightly higher when compared to the 60 L/min. The FPF with the medium sized carrier greatly increased at 90 L/min.

The small, medium and large lactose carrier formulations were different in their sieve size range (median): 20–30(21), 30–71(58) and 71–90(76) µm, respectively. It was of interest that, the medium sized lactose carrier formulation tended to provide the best performance formulation. It had the widest sieve size range of 30–71(58) µm. The wide size range of the carrier size might have some effect on the aerosolization performance. The smaller particles in the wide size range of the dispersion carrier could modify the surface properties of the larger carrier and loosen adhesion of the agglomerate formulation. It was reported that the fine lactose portion improved the efficacy of the formulation [34]. However, the mechanism of this observation was not provided, hence it needs more investigation.

The MMAD was in the range of 4–6 µm and when the flow-rate increased in both devices, the MMAD was slightly lower. The Inhalator® is a high resistance device and gave a smaller MMAD than that for the Cyclohaler® which is a medium resistance device at all flow-rates. The MMAD for the Cyclohaler® was slightly larger at a flow-rate of 30 L/min and decreased when the flow-rate was increased from 30 to 90 L/min (Fig. 3A). The Inhalator® operated at 30 and 60 L/min had a comparable MMAD with all carrier sizes whereas the MMAD at 90 L/min was slightly lower and with the medium sized carrier had the lowest MMAD (Fig. 3B).
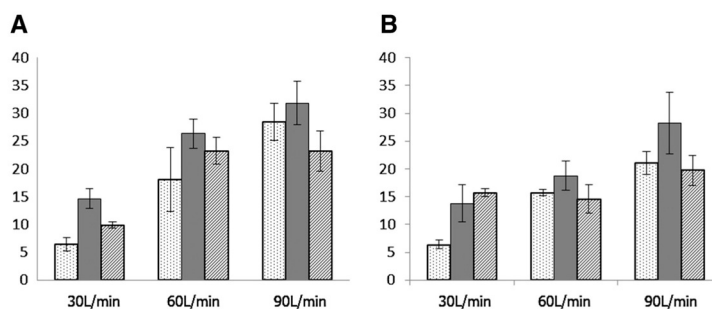
Fig. 2. The percentage Fine Particle Fraction (%FPF) of the Cyclohaler® (A) and the Inhalator® (B) at flow-rates of 30, 60 and 90 L/min with the small (▱), medium (▪) and large (▨) lactose carriers.
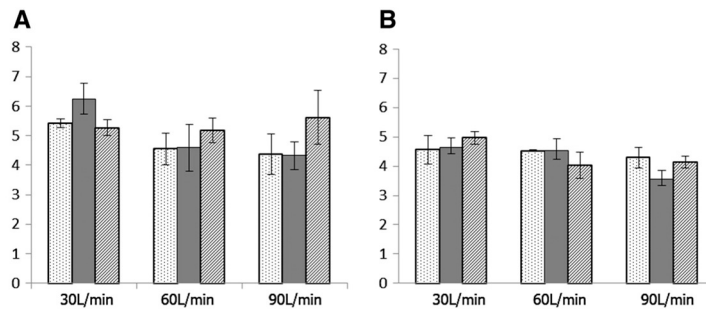
Fig. 3. MMAD (μm) of the Cyclohaler® (A) and the Inhalator® (B) at flow-rates of 30, 60 and 90 L/min with the small (▨), medium (■) and large (▨) lactose carriers.

3.3. Computational simulation

Fig. 4A shows that the Cyclohaler® is a unit-dose dry powder inhaler device. The Cyclohaler® consists of a three part mouthpiece tube (A), cyclone chamber (B) and capsule holder (C). The dry powder formulation was filled into no. 3 capsules and the capsule was placed in a capsule holder. The press button on the device was used to release needles to pierce holes on the capsule. The dry powder was then released through the holes. After that the patient inhaled the medication through the mouthpiece. During inhalation the medication powder was dispersed and aerosolized along the device.

The Inhalator® (Fig. 4B) is also a unit-dose device which has a relatively simple design being a straight tube with an eclipse bell-shaped mouthpiece (part A). The medication capsule holder is in the lower part (part C) of the device. The needles are released to pierce the capsule on the middle of the capsule. The grid is in part B that is located between the straight tube part and the conical part. Hence the medication powder is released and deagglomerated to produce a fine particle of aerosols along the device. Total mesh node in the Cyclohaler® and Inhalator® was 739,377 and 581,917 nodes, respectively. The mesh independent was tested using variation of integral strain rate. The mesh node in the Cyclohaler® increased from 739,377 to 837,519, 948,590, 985,855 and 1,474,015 from the decrease of the maximum element size at 10^{-4} m on each step. The Inhalator® mesh increased from 581,917 to 797,514, 835,645, 972,237 and 1,345,437 nodes from a similar methodology. It was found that the integral strain rate changed less than 5% which indicated independency from the mesh [35]. The velocity streamlines of the airflow in the Cyclohaler® and Inhalator® are shown in Fig. 5. In the Cyclohaler®, the flow had input from two inlets on the side of the cyclone chamber (Fig. 5A). The air inlet channels are configured in a tangent form to create a cyclone like effect and make a swirly flow in the cyclone chamber with a velocity of 4–5.5 m/s. The airflow was transitioned to the mouthpiece tube, which decreased the velocity to 1.37–2.8 m/s. On the other hand, the flow that entered the Inhalator® device had a smaller inlet tube and changed direction when passing the cross grid (1 mm thick and 1 mm width) (Fig. 5B). The airflow velocity was very high initially (around 44 m/s) at 90 L/min. It related to inlet

channel cross-sectional area. The airflow velocity then decreased dramatically along the device to the mouthpiece (4–7 m/s). Moreover, the grid in the Cyclohaler® and Inhalator® showed similar effects to the flow pattern. It changed the airflow from a swirly or chaotic flow into a linear stream along the mouthpiece. Previous research had also demonstrated that the role of the grid was to fix the flow in the Cyclohaler® [36].

The electrostatic charges during the aerosolization ranged from 0.1 to 0.3 nC/mg from a 30–90 L/min flow-rate. Thus electrostatic charge effects can be omitted due to the magnitude of the electrostatic charges being very low and it does not have any significant role in the aerosolization performance [37].

The impaction counts per injected particle varied with the flow-rate. Increasing the flow-rate led to a higher impaction count per injected particle. In the Cyclohaler® the impaction events were higher when the flow-rate increased, whereas the impaction showed little difference at the same flow-rate with the small, medium and large carriers (Table 4). The impaction of the device particles in the Inhalator® did not relate well to the flow-rate and carrier sizes. However the probability of the analysis for the variance (ANOVA) of deagglomeration for the small, medium and large carriers with 30 L/min flow-rates indicated that the carrier size had a minimal effect on the probability of deagglomeration at a low flow-rate (Table 4). At the 60 and 90 L/min flow-rate carrier sizes had dramatic effects on the probability of deagglomeration especially for the Inhalator® device. The explanation is that at 30 L/min the momentum carried by the different particle size was not significantly distinct. Thus the probability of deagglomeration was not significantly different. However, there was a fluid shear force that could affect the magnitude of deagglomeration.

The probability of deagglomeration by the z-position in the Cyclohaler® is shown in Fig. 6. The probability of deagglomeration is high in the mixing chamber and transitional zone. Most impaction occurred near the pierced holes on the capsules (release point) and the mixing chamber whereas there was a lowering of impaction in the mouthpiece zone. It supported the finding of Zhou et al. that changing mouthpiece length doesn't show any significant effect on the aerosolization of Foradil from the Aerolizer® [26]. This evidence supported
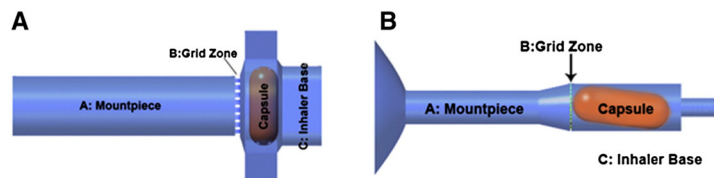
Fig. 4. Cyclohaler® (A) and Inhalator® (B) geometry and reference position.
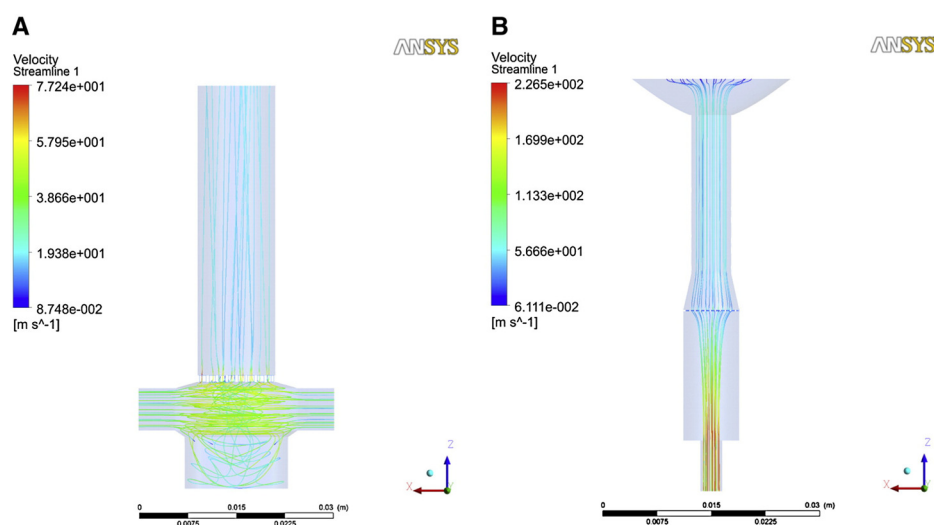
Fig. 5. Velocity streamline of the Cyclohaler® (A) and the Inhalator® (B) at 90 L/min.

the probability that particle deagglomeration not only depended on the particle impaction count but also on the impaction energy. One key factor to design a high performance dry powder inhaler device is to increase the frequency of impaction. A higher flow-rate leads to a higher degree of particle deagglomeration because the high flow-rate provides more input of energy to the particle system. The relative standard deviations of impaction per particle were around 0.6–1 and this implied that the particle–wall impaction distribution was better than in the Inhalator® due to the swirling flow in the device. The particle size showed no statistically significant effect on the degree of deagglomeration at the flow rate of 30 L/min in the Cyclohaler® and Inhalator® (Table 4). However at 60 and 90 L/min the carrier particle size played an important role on the degree of deagglomeration with the medium and large carriers and gave a better dispersion performance than the small carrier. One explanation could be that at a low flow-rate, the energy from impaction was not high enough to create any significant break-up of drug-carrier agglomerate. This can be further clarified using an atomic force microscope to directly measure the adhesive force between the drug and carrier [16,38]. However, when the probability of deagglomeration was compared to the %FPF it did not show any correlation because the simulation was done only in the DPI device. Yet the induction port of the ACI from the USP may introduce deagglomeration of the powder and lead to a higher breakup potential [39].

The Inhalator® with a cross sectional grid area that was used under the assumption that the grid would provide more impaction by changing the air flow pattern in the Inhalator®. The impaction of particles in the Inhalator® with a cross grid occurred at around 13,000 to 17,000 impactions per 200 injected particles. This is similar to that of the Cyclohaler® that has a cyclone-like design (Table 3). This result supports the assumption that the grid is a key element to improve wall–particle impaction in the low vorticity inhaler device. The probability of the particle deagglomeration in the Inhalator® device is high at all flow-rates and with all the three carrier sizes. The probability of impaction almost reaches 1.00 due to the high impaction energy (Fig. 6A). However, the relative standard deviations of the impaction per particle were extremely large (around 1.8 to 6.6). It means that some particles impacted more frequently than some others because the simulation in the grid of the Inhalator® has a large void space and the air-flow is almost straight forward along the device, so some particles passed through the void space and faced fewer impactions than the particles that went straight to the grid.

The TKE is the mean kinetic energy per unit mass associated with eddies in the turbulent flow. Physically, the TKE is characterized by the measured root-mean-square (RMS) velocity fluctuations. TKE is directly related to the magnitude of the turbulence [40]. The TKE in the Cyclohaler® ranges (mean) from 1–30 (2.56) J kg^{-1},

Table 3
The impaction count from a stochastic simulation of the Cyclohaler® and Inhalator®.

Parameters	Small carrier			Medium carrier			Large carrier		
	30 L/min	60 L/min	90 L/min	30 L/min	60 L/min	90 L/min	30 L/min	60 L/min	90 L/min
Cyclohaler®									
Total impaction[b]	10,299	13,651	18,588	10,110	13,594	17,491	10,502	13,881	17,384
Average I/P[a]	21	27	37	20	27	35	21	28	35
SD	13	23	24	13	23	22	15	28	21
Inhalator®									
Total impaction[b]	13,575	13,919	16,174	13,786	16,035	16,995	13,045	13,671	15,927
Average I/P[a]	27	28	32	26	32	34	28	27	26
SD	48	88	104	53	197	225	80	77	58

[a] I/P = impactions/particle.
[b] Count per 200 particles.

Table 4

Analysis of variance (ANOVA) of deagglomeration probability in the Cyclohaler® and Inhalator® for the small, medium and large carriers at 30, 60 and 90 L/min flow-rates, respectively.

Flow-rate group	P-value	
	Cyclohaler®	Inhalator®
30 L/min	0.28945	0.8633
60 L/min	0.02079	0.0033
90 L/min	0.02282	0.0090

Significant level $\alpha = 0.05$.

$2–110$ (9.7) J kg^{-1} and $5–220$ (22.4) J kg^{-1} at the flow-rates of 30, 60 and 90 L/min, respectively. At the flow-rate of 30 L/min, the TKE is relatively low compared to that at 60 and 90 L/min. The TKE occurs mostly at the inlet and cyclone part of the Cyclohaler® due to the rapid change of airflow direction and airflow velocity as visualized in the velocity streamline and contour plot of the TKE (Fig. 7A). In this case an increase of the TKE elevated the level of particle impaction because of the rapid swirling of the airflow in the cyclone part of the device that introduced a greater probability of impaction–deagglomeration of the particles on the wall. Linear regression between FPF and TKE showed a strong correlation at all carrier sizes ($R^2 = 0.735–0.998$). The relationship between TKE and FPF was a direct variation; i.e., as TKE increases, FPF proportionally increases (Fig. 8A). The large carrier formulation gave the lowest correlation coefficient (0.735) because %FPF reaches plateau from 60 L/min to 90 L/min. The slope of FPF and TKE linear curve in Cyclohaler® for fine, medium and large lactose carriers was 1.0076, 0.7858 and 0.604, respectively. The fine and medium lactose carrier

formulations sharply responded to the TKE when compared to a large lactose carrier formulation. This indicated that the FPF in the small carrier size formulation reacted more strongly to the TKE than that occurred with the larger carrier formulation. MMAD also showed a moderate correlation with TKE (0.559–0.862) (Fig. 8B). The MMAD and TKE had an inverse relationship; i.e., when TKE increased, MMAD proportionally decreased.

For the Inhalator® the TKE range (mean) values varied from 0.5–263.6 (23.4) J kg^{-1}, 1.3–1009.0 (87.3) J kg^{-1} and 2.3–2236.0 (190.1) J kg^{-1} at the flow-rates of 30, 60 and 90 L/min, respectively. The magnitude of the TKE in the Inhalator® was about 10 times higher than in the Cyclohaler®. The TKE mainly occurred around the capsule chamber and the grid where the air-flow changed its direction (Fig. 7B). When we considered the probability of particle deagglomeration it almost reached 1 in all positions of the device (Fig. 6A). This was related to the high kinetic energy of the particles in the system and was also correlated with the MMAD (Fig. 3A) that decreased as the probability of particle deagglomeration increased. The relationship between FPF and TKE was observed (Fig. 8C). FPF and TKE have a linear correlation with R^2 between 0.692 and 0.998. The slope of FPF and TKE linear curve in the Inhalator® for fine, medium and large lactose carriers was 0.2316, 0.2334 and 0.0689, respectively. This indicated that the %FPF in the fine and medium sized carriers also sharply responded to TKE than that of the large lactose carrier. The response of FPF to TKE in the Inhalator® was lower than in the Cyclohaler® because the initial TKE at 30 L/min in the Inhalator® was significantly higher than the Cyclohaler®. Linear correlation between MMAD and TKE has R^2 around 0.577–0.894.

It showed fair to medium-high correlation between TKE and MMAD. The MMAD and TKE also had a reverse relationship. The relation trends were similar in the Cyclohaler® device.
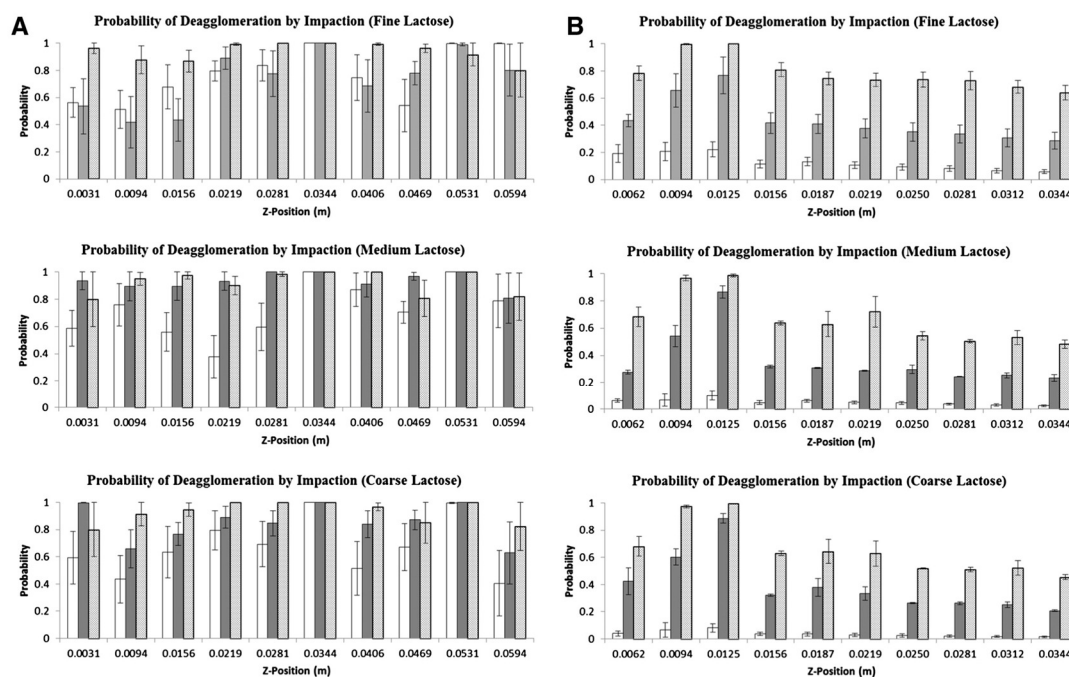
Fig. 6. Probability of deagglomeration by impaction in the Inhalator® (A) and the Cyclohaler® (B) at 30 (□), 60 (■) and 90 (▨) L/min (z-position is a center of stratums, each strata is 1 in 10 of device z length).
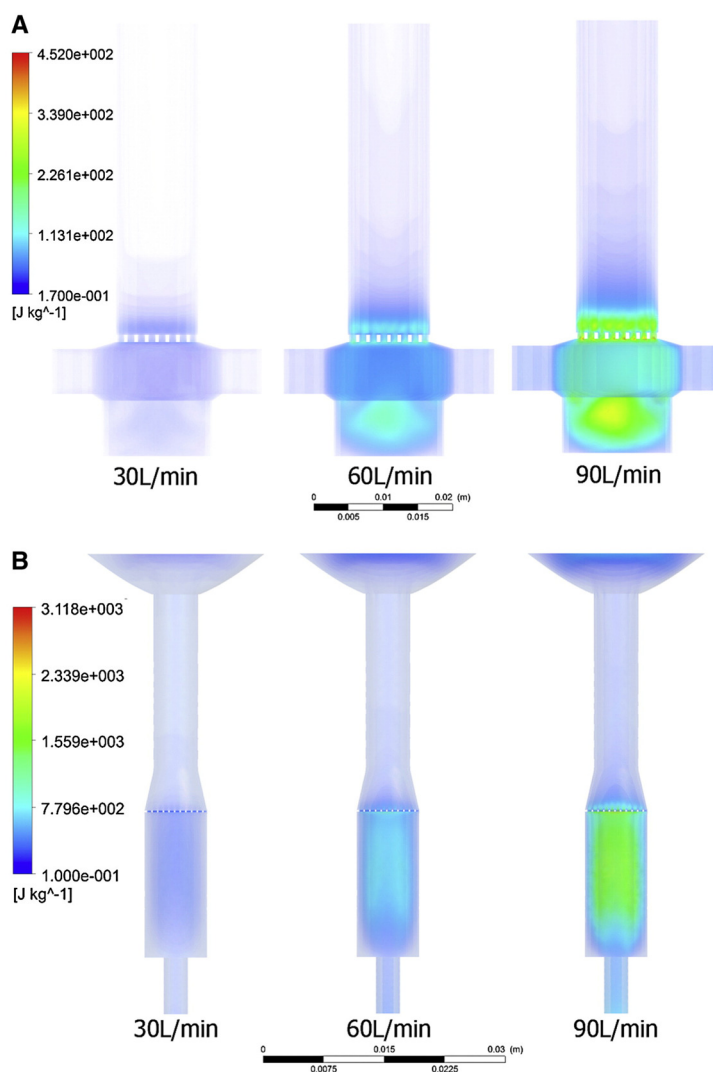
Fig. 7. Contour plot of TKE in the Cyclohaler® (A) and the Inhalator® (B) at 30, 60 and 90 L/min (flow direction is upward).

There is an assumption that %FPF in the fine and medium sized carriers also highly responded more to the TKE than that in the large lactose carrier. The larger size carrier formulation of the drug particles was readily released from the carrier surface of a lower TKE. Thus, an increase of the TKE had a little effect on the improvement of the FPF in the larger carrier. Whereas, the smaller carrier formulation initially yielded a lower FPF than the larger carrier at a low TKE. The increment of the TKE in the small carrier at the same rate as in the larger carrier steeply improved the FPF. Nevertheless the turbulence kinetic energy, impaction frequency and impaction kinetic energy had to be taken into consideration simultaneously [41].

The TKE also indicated the amount of energy used when the fluid interacts with the particles and causes fluid dynamic shearing of the particles. More energetic particle impaction means an increase of particle deagglomeration and more fluid shearing on the carrier-drug particle agglomerates so increases the probability of drug particles detaching from the carrier surface. According to the work of Voss and Finlay, turbulence also plays a key role in the aerosolization process [24]. Thus, the Inhalator® has a higher probability of detachment of the drug particles from the carrier surface than the Cyclohaler® as determined by fluid dynamic shearing.

Probability of deagglomeration directly related TKE; i.e., as TKE increased, probability of deagglomeration proportionally increased. Both the Cyclohaler device (Fig. 9A) and the Inhalator® device (Fig. 9B) showed a good linear correlation with $R^2 > 0.8$. The TKE was probed along the longitudinal length of the Cyclohaler® device. It was found that the TKE at a constant flow rate of 60 L/min varied with the longitudinal position of the Cyclohaler® (Fig. 10A). TKE was the highest around
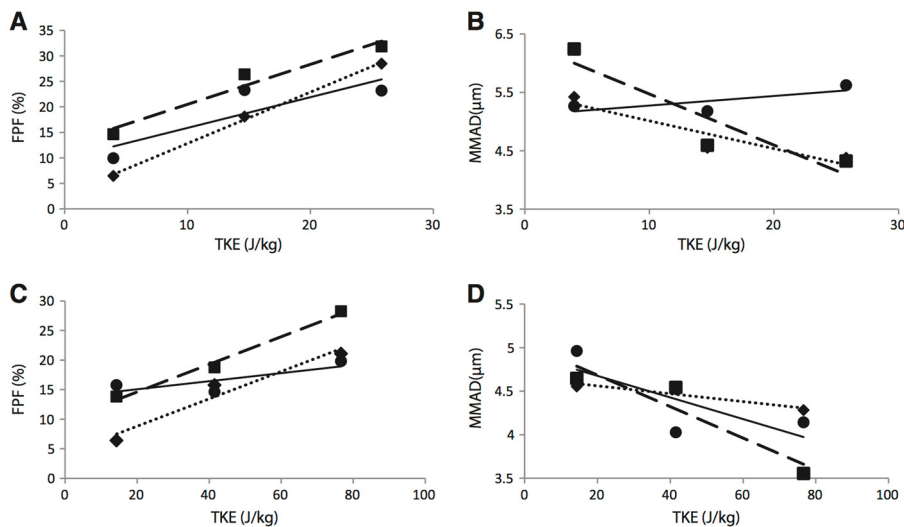
Fig. 8. Correlation of FPF to TKE and MMAD in Cyclohaler device (A, B) and Inhalator® device (C, D) with fine (♦, dotted line), medium (■, dash line) and large (●, solid line) lactose carrier formulations.

a position of 1.875 mm in the upper part of the device chamber and grid. The TKE had a good correlation ($R^2 = 0.999$) with the impaction energy and the probability of deagglomeration by impaction (Fig. 10B). It can be explained that the TKE was converted to a particle–wall impaction energy in combination with the particle–wall impaction frequency and the probability of deagglomeration.

4. Conclusion

The particles deagglomerated in two different ways; by aerodynamic shear dispersion and mechanical impaction deagglomeration, in that respective order. The aerodynamic shear force creates stress on particle agglomeration and separates them. We found that the TKE was a key parameter that can describe the aerodynamic shear force. If the TKE overcomes the interparticulate force, it will break the agglomerated particles. The TKE can be increased by adding a swirly flow as in the Cyclohaler® and using the narrow flow-path as in the Inhalator®. The Cyclohaler® used its cyclone-like design that consists of a tangential flow across the axial flow. It changes the particle trajectory by a swirly movement and many particles impact on the wall of the device. In addition, a swirly flow generates a more turbulent kinetic energy in the flow. In contrast, the Inhalator® has a straight tube design and grid. The grid obstructs some airflow, so the air and particle rapidly change their directions. The high resistance of the Inhalator® maximizes the air velocity and is the cause of the energetic impaction and shear force. However, the inertial impaction on the airways of a high velocity particle will cause some loss of the drug. A high performance dry powder inhaler device can be designed based on the cyclone chamber design of the Cyclohaler® and the grid design of the Inhalator® as a guideline because it provides a balance between the resistance of the device and the dispersion performance of the deagglomerated particles. The TKE plays a significant role in the particle deagglomeration and the FPF.
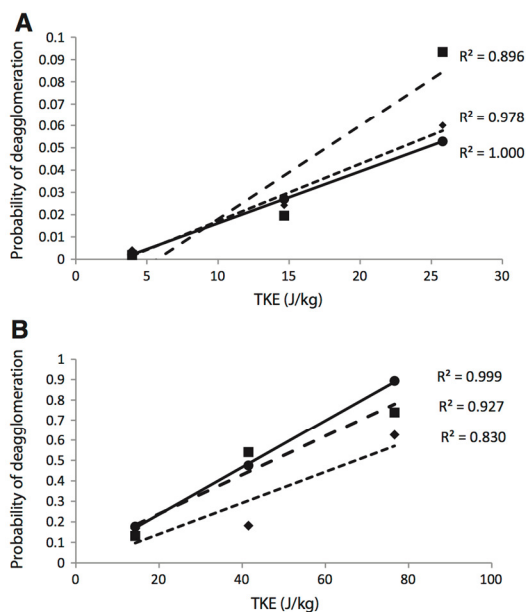
Fig. 9. Correlation of TKE and probability of deagglomeration in Cyclohaler device (A) and Inhalator® device (B) with fine (♦, dotted line), medium (■, dash line) and large (●, solid line) lactose carrier formulations.

Fig. 10. TKE (bar) and impaction (line) energy along longitudinal length of the Cyclohaler® (A), correlation of TKE to impaction energy (▲, solid line) and probability of deagglomeration by impaction (●, dash line) (B) at 60 L/min, medium sized lactose carriers.

References

[1] D.I. Daniher, J. Zhu, Dry powder platform for pulmonary drug delivery, Particuology 6 (2008) 225–238.

[2] M.S. Coates, H.K. Chan, D.F. Fletcher, H. Chiou, Influence of mouthpiece geometry on the aerosol delivery performance of a dry powder inhaler, Pharm. Res. 24 (2007) 1450–1456.

[3] M.S. Coates, H.K. Chan, D.F. Fletcher, J.A. Raper, Effect of design on the performance of a dry powder inhaler using computational fluid dynamics. Part 2: air inlet size, J. Pharm. Sci. 95 (2006) 1382–1392.

[4] M.S. Coates, D.F. Fletcher, H.K. Chan, J.A. Raper, Effect of design on the performance of a dry powder inhaler using computational fluid dynamics. Part 1: grid structure and mouthpiece length, J. Pharm. Sci. 93 (2004) 2863–2876.

[5] W.P. Adams, S.L. Lee, R. Plourde, R.A. Lionberger, C.M. Bertha, W.H. Doub, J.-M. Bovet, A.J. Hickey, Effects of device and formulation on in vitro performance of dry powder inhalers, AAPS J. 14 (2012) 400–409.

[6] M.P. Timsina, G.P. Martin, C. Marriott, D. Ganderton, M. Yianneskis, Drug delivery to the respiratory tract using dry powder inhalers, Int. J. Pharm. 101 (1994) 1–13.

[7] AstraZeneca, Pulmicort Flexhaler(R) Prescribing Information, AztraZeneca AB, Södertälje, Sweden, 2010. 5.

[8] Y. Zhou, Y.S. Cheng, Particle deposition in first three generations of a human lung cast, J. Aerosol Sci. 31 (2000) 140–141.

[9] J. Visser, Van der Waals and other cohesive forces affecting powder fluidization, Powder Technol. 58 (1989) 1–10.

[10] S.S. Desai, A.A. Aher, P.T. Kadaskar, Methods for reduction of cohesive forces between carrier and drug in DPI formulation, Drug Dev. Ind. Pharm. 39 (2013) 1589–1598.

[11] K.S. Hayden, K. Park, J.S. Curtis, Effect of particle characteristics on particle pickup velocity, Powder Technol. 131 (2003) 7–14.

[12] X. Dou, Y. Mao, Y. Zhang, Effects of contact force model and size distribution on microsized granular packing, J. Manuf. Sci. Eng. 136 (2014) (021003-021003).

[13] K.T. Chow, K. Zhu, R.B.H. Tan, P.W.S. Heng, investigation of electrostatic behavior of a lactose carrier for dry powder inhalers, Pharm. Res. 25 (2008) 2822–2834.

[14] S. Karner, M. Maier, E. Littringer, N.A. Urbanetz, Surface roughness effects on the tribo-charging and mixing homogeneity of adhesive mixtures used in dry powder inhalers, Powder Technol. 264 (2014) 544–549.

[15] G. Calvert, M. Ghadiri, R. Tweedie, Aerodynamic dispersion of cohesive powders: a review of understanding and technology, Adv. Powder Technol. 20 (2009) 4–6.

[16] P. Begat, D.A.V. Morton, J.N. Staniforth, R. Price, The cohesive–adhesive balances in dry powder inhaler formulations II: influence on fine particle delivery characteristics, Pharm. Res. 21 (2004) 1826–1833.

[17] C. Kleinstreuer, Z. Zhang, Laminar-to-turbulent fluid–particle flows in a human airway model, Int. J. Multiphase Flow 29 (2003) 271–289.

[18] C. Kleinstreuer, Z. Zhang, Z. Li, W.L. Roberts, C. Rojas, A new methodology for targeting drug-aerosols in the human respiratory system, Int. J. Heat Mass Transfer 51 (2008) 5578–5589.

[19] Y. Zhang, W.H. Finlay, E.A. Matida, Particle deposition measurements and numerical simulation in a highly idealized mouth–throat, J. Aerosol Sci. 35 (2004) 789–803.

[20] P.W. Longest, Y.J. Son, L. Holbrook, M. Hindle, Aerodynamic factors responsible for the deaggregation of carrier-free drug powders to form micrometer and submicrometer aerosols, Pharm. Res. 30 (2013) 1608–1627.

[21] W. Wong, D.F. Fletcher, D. Traini, H.-K. Chan, J. Crapper, P.M. Young, Particle aerosolisation and break-up in dry powder inhalers 1: evaluation and modelling of venturi effects for agglomerated systems, Pharm. Res. 27 (2010) 1367–1376.

[22] J. Gac, T.R. Sosnowski, L. Gradon, Turbulent flow energy for aerosolization of powder particles, J. Aerosol Sci. 39 (2008) 113–126.

[23] C.G. Ball, M. Uddin, A. Pollard, High resolution turbulence modelling of airflow in an idealised human extra-thoracic airway, Comput. Fluids 37 (2008) 943–964.

[24] A. Voss, W.H. Finlay, Deagglomeration of dry powder pharmaceutical aerosols, Int. J. Pharm. 248 (2002) 39–50.

[25] C. Thornton, L. Liu, How do agglomerates break? Powder Technol. 143–144 (2004) 110–116.

42

[26] Q.T. Zhou, Z. Tong, P. Tang, M. Citterio, R. Yang, H.-K. Chan, Effect of device design on the aerosolization of a carrier-based dry powder inhaler—a case study on Aerolizer® Foradile®, AAPS J. 15 (2013) 511–522.

[27] Y. Guo, K.D. Kafui, C.-Y. Wu, C. Thornton, J.P.K. Seville, A coupled DEM/CFD analysis of the effect of air on powder flow during die filling, AIChE J. 55 (2003) 49–62.

[28] T. Srichana, R. Suedee, P. Srisudjai, Application of spectrofluorometry for evaluation of dry powder inhalers in vitro, Pharmazie 58 (2003) 125–129.

[29] R.F. Oliveira, S.F.C.F. Teixeira, L.F. Silva, J.C.F. Teixeira, H. Antunes, Development of new spacer device geometry: a CFD study (part I), Comput. Method Biomed. 15 (2012) 825–833.

[30] P.W.S. Heng, L.H. Chan, L.T. Lim, Quantification of the surface morphologies of lactose carriers and their effect on the in vitro deposition of salbutamol sulphate, Chem. Pharm. Bull. 48 (2000) 393–398.

[31] Fluent Inc., Modeling Discrete Phase, FLUENT 6.3 User's Guide, Fluent Inc., 2005. 22–23.

[32] L. Vogel, W. Peukert, Breakage behaviour of different materials—construction of a mastercurve for the breakage probability, Powder Technol. 129 (2002) 101–111.

[33] T. Suwandecha, K. Assawadarakorn, T. Srichana, Feasibility studies of using a tobacco pipe as a dry powder inhaler device, Thail. J. Pharm. Sci. 36 (2012) 1–11.

[34] T. Srichana, G.P. Martin, C. Marriott, On the relationship between drug and carrier deposition from dry powder inhalers in vitro, Int. J. Pharm. 167 (1998) 13–23.

[35] Q.T. Zhou, Z. Tong, P. Tang, R. Yang, H.-K. Chan, CFD analysis of the aerosolization of carrier-based dry powder inhaler formulations, AIP Conf ProcAIP Publishing, Sydney, Australia, 2013.

[36] Z. Tong, B. Zheng, R. Yang, A. Yu, H. Chan, CFD–DEM investigation of the dispersion mechanisms in commercial dry powder inhalers, Powder Technol. 240 (2013) 19–24.

[37] H. Adi, P.C. Kwok, J. Crapper, P.M. Young, D. Traini, H.K. Chan, Does electrostatic charge affect powder aerosolisation? J. Pharm. Sci. 99 (2010) 2455–2461.

[38] P.M. Young, M.J. Tobyn, R. Price, M. Buttrum, F. Dey, The use of colloid probe microscopy to predict aerosolization performance in dry powder inhalers: AFM and in vitro correlation, J. Pharm. Sci. 95 (2006) 1800–1809.

[39] P. Tang, P. Kwok, Z. Tong, R. Yang, J. Raper, H.-K. Chan, Does the United States pharmacopeia throat introduce de-agglomeration of carrier-free powder from inhalers? Pharm. Res. 29 (2012) 1797–1807.

[40] W.K. George, The Turbulence Kinetic Energy, Lectures in Turbulence for the 21st Century, Department of Thermo and Fluid Engineering, Chalmers University of Technology, Göteborg, Sweden, 2005. 59–70.

[41] Q.T. Zhou, P. Tang, S.S.Y. Leung, J.G.Y. Chan, H.-K. Chan, Emerging inhalation aerosol devices and strategies: where are we headed? Adv. Drug Deliv. Rev. (2014) (in Press).

PAPER 2

Computer-aided Design of Dry Powder Inhalers Using Computational Fluid Dynamics to Assess Performance

(Manuscript accepted to publish in *Pharmaceutical Development and Technology*)

44

05-Sep-2014

Dear Professor Srichana:

Ref: Computer-aided Design of Dry Powder Inhalers Using Computational
Fluid Dynamics to Assess Performance

I am pleased to accept your paper for publication in Pharmaceutical
Development and Technology. It will now be forwarded to the publisher for
copy editing and typesetting.

You will receive proofs for checking, and instructions for transfer of
copyright in due course.

The publisher also requests that proofs are checked and returned within 48
hours of receipt.

Thank you for your contribution to Pharmaceutical Development and
Technology and we look forward to receiving further submissions from you.

Sincerely,

Michael J. Akers, Ph.D.
Editor-in-Chief
Pharmaceutical Development and Technology

Visit www.informahealthcare.com and sign up for free eTOC alerts to all
Informa Pharmaceutical Science journals

RESEARCH ARTICLE

Computer-aided design of dry powder inhalers using computational fluid dynamics to assess performance

Tan Suwandecha[1], Wibul Wongpoowarak[1], and Teerapol Srichana[2]

[1]Faculty of Pharmaceutical Sciences, Prince of Songkla University, Songkhla, Thailand and [2]Faculty of Pharmaceutical Sciences, NANOTEC-PSU Drug Delivery System Excellence Center, Prince of Songkla Univesity, Songkhla, Thailand

Abstract

Dry powder inhalers (DPIs) are gaining popularity for the delivery of drugs. A cost effective and efficient delivery device is necessary. Developing new DPIs by modifying an existing device may be the simplest way to improve the performance of the devices. The aim of this research was to produce a new DPIs using computational fluid dynamics (CFD). The new DPIs took advantages of the Cyclohaler® and the Rotahaler®. We chose a combination of the capsule chamber of the Cyclohaler® and the mouthpiece and grid of the Rotahaler®. Computer-aided design models of the devices were created and evaluated using CFD. Prototype models were created and tested with the DPI dispersion experiments. The proposed model 3 device had a high turbulence with a good degree of deagglomeration in the CFD and the experiment data. The %fine particle fraction (FPF) was around 50% at 60 L/min. The mass median aerodynamic diameter was around 2.8–4 µm. The FPF were strongly correlated to the CFD-predicted turbulence and the mechanical impaction parameters. The drug retention in the capsule was only 5–7%. In summary, a simple modification of the Cyclohaler® and Rotahaler® could produce a better performing inhaler using the CFD-assisted design.

Introduction

Pharmaceutical inhalers have the potential to treat not only lung diseases such as asthma, they are also excellent devices for the systemic delivery of drugs. The insulin dry powder inhaler (DPI) is an example of a systemic drug delivery device that avoids injection[1]. At present there are three major types of inhalers used to disperse and aerosolize drugs: nebulizers, pressurized metered-dose inhalers (pMDIs) and DPIs. The most important aspect for efficient pulmonary drug delivery is to produce particles that are aerodynamically smaller than 5 µm so they can reach the lower parts of the lungs[2]. DPI formulations usually consist of a micronized drug alone or as a blend. Relatively larger coarse carrier particles may be added either as a diluent or carrier[3]. It is very important to optimize the flow properties, dispersibility and aerosolization performance to achieve a desired dose to the target organ[4]. When patients operate an inhaler device, their inspiratory flow is the primary energy source needed to detach the drug and to disperse any agglomerated carrier particles[5]. Because of their size the larger carrier particles themselves deposit in the oropharyngeal regions, whereas the drug particles flow with the air stream and are deposited in the lower parts of the lungs. The efficiency of a DPI is measured by assessing the distribution of the aerodynamic sizes of the particles using multistage impaction equipment (Andersen cascade impactor) or multistage liquid impingement equipment (multistage liquid impinger). Two main efficiency parameters are obtained from the aerodynamic size distribution: the mass median aerodynamic diameter (MMAD) (i.e. is the effective size of the particles in the air flow) and the fine particle fraction (FPF) (i.e. the fraction of particles that has an aerodynamic size of less than 5 microns)[6]. The MMAD is calculated by linear regression of the log-normal aerodynamic size distribution, as shown in Figure 1[7]. In addition, the geometric standard deviation also describes the span of the size distribution. There are three main types of DPIs that can be differentiated by their method of dosing. The simplest type is a single-unit dose device in which the DPI formulation is filled into a capsule and the patient manually loads the capsule into the device[8]. Some devices now allow patients to preload several capsules in the inhaler for convenience. The second type delivers a multiple unit dose in which an accurately weighed powder formulation is pre-filled into a blister or disk pack[9]. When the patient operates the device, the mechanical processes break the blister or disk once per use. The third type has a bulk reservoir with a built-in metering apparatus. A large amount of powder is filled into a bulk reservoir container and the metering mechanism portions out a dose for each actuation. This multiple dose type inhaler has an inferior stability and consistency of dosage compared to the single-unit dose or multiple unit dose inhalers[10].

The three main factors governing the efficiency of the DPIs are: the formulation of the dry powder, the inspired flow rate and the design of the device. The dry powder formulation determines the strength of the agglomeration between the drug–drug,

Address for correspondence: Teerapol Srichana, Faculty of Pharmaceutical Sciences, Drug Delivery System Excellent Center, Prince of Songkla Univesity, Songkhla, Thailand. E-mail: teerapol.s@psu.ac.th
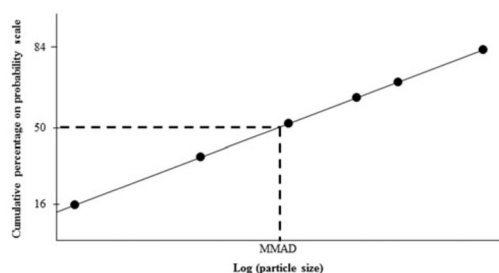
Figure 1. Plot of cumulative percentage of mass less than stated aerodynamic diameter (probability scale) versus aerodynamic diameter (log scale) (Redrawn from USP 34/NF 29, 2011).

drug–carrier and carrier–carrier particles. Lowering the particle adhesion force leads to an easier dispersion[11]. The DPIs are passive devices that lack an internal energy source to aerosolize the powder. They rely on the inhalation airflow as the primary force to overcome the inter-particle force of a dry power formulation. Increasing the inhalation flow rate adds more energy to the system and increases the dispersion performance[12].

The design of a device is also an important factor that impacts on its aerosolization performance[13]. Recent commercial and research devices are able to produce a FPF in the range of 10–70%[10]. Several research groups have worked on the design of the Aerolizer® using computational fluid dynamics (CFD) in conjunction with experiments using various mouthpiece geometries, air inlet sizes and grid structures. The results have indicated that only small modifications to the geometry of the device can have a large effect on the aerosolization performance[14–16]. The geometry of the device controls the air flow dynamics within the device that affects the airflow resistance, distribution of turbulent flow, fluid drag forces that act on the particles, particle trajectory and impaction patterns[17]. The deagglomeration magnitude increases with the aerodynamic shear, the collision frequency and the impaction energy of the particles. A variety of device designs have been adapted to improve these parameters[5,18]. Previously some DPIs had a high airflow resistance design that increases the deagglomeration force of the particles that emerge from the mouthpiece in the hope that they will improve the deposition in the lower lungs[19]. However, a device with a high resistance requires a high inhalation effort that is practically difficult for patients with impaired lung function to achieve[20]. There has been some evidence that a high air flow resistance is not necessary to improve the performance of the DPIs[21]. Some early low-resistant device designs, such as the Spinhaler® and the Rotahaler®, employed a grid to intensify the turbulence but lowered the device resistance[10]. However, both devices still produced a low %FPF of around 9–10%[22,23]. Another approach was to design a cyclone chamber with a mesh that created a swirly turbulent flow inside the device that enhanced the dispersion of the powder. The Turbuhaler® is a multiple-dose device that produces an FPF of up to 27% with an air-flow of 57 LPM[24]. In some capsule-based single-dose device, a capsule chamber was designed that produced a rotation of the capsule or developed sufficient vibrations to assist the deagglomeration of the powder such as the Cyclohaler®. A FPF of up to 25% at 60 LPM was achieved using the Cyclohaler®[5]. From the above information, designing a high-performance DPI requires a careful optimization of many variables. Computational-assisted design has proved to be a very useful tool for investigating dynamic processes in the device. Recently, discrete element modeling (DEM) has been used to

dynamically simulate the particle de-agglomeration processes. It has provided an acceptable prediction of particle aerosolization when coupled with CFD[25]. However, this method requires a high computational power[26]. Tong et al. used CFD to demonstrate that narrowing the air inlet channel of the Aerolizer® device significantly improved FPF[27].

The aim of this research was to develop new inhaler devices based on the currently commercially available devices. The development process employed a computer-aided design together with an investigation on the particle aerodynamics, and the behavior of the particles during the aerosolization process.

Materials and methods

Computational modeling and rapid prototyping of inhaler devices

The inhalers were sketched and modeled using the CAD program Autodesk® Inventor® (Autodesk, Inc, San Rafael, CA). The internal geometries of the devices were exported for further computational fluid dynamic processing. The prototype devices were created by extending a wall from the internal geometry. The wall thickness was set at 2 mm. The prototypes were printed using a fuse deposit rapid prototyping machine, MakerBot® Replicator® 2 (MakerBot Industries, Brooklyn, NY). The printing material was white acrylonitrile butadiene styrene (ABS) plastic. The prototypes were sanded to smooth their surfaces.

CFD analysis

Computational fluid dynamics

The CFD simulation was solved using Ansys Fluent® 14 (ANSYS, Inc.; Cecil Township, PA). All inhaler device models were meshed to generate the computational elements. The mesh convergence test was performed until the turbulent kinetic energy (TKE) deviated of less than 5%. The fluid dynamic simulation was based on the momentum, mass and energy conservation (Navier–Stoke equation). Due to the tracking of complex particles the CFD computations required high-computational powder, so only the simple flow analysis and particles tracking were calculated[28]. The turbulence model was the RNG k-ε where k and ε described the TKE and the turbulent dissipation rate, respectively. Second-order upwind schemes were applied to discretize the partial differential equations of a momentum, TKE and turbulent dissipation rates. A semi-implicit method for a pressure linked equation (SIMPLE) algorithm was used for the coupling of the mass and momentum equations[29]. The mouthpiece was set as the velocity inlet boundary condition and the air inlet orifice was set as the pressure inlet boundary condition. Simulation condition was set as standard ambient temperature and pressure (SATP) condition. The calculation was iterated until the residual error was less than 10^{-3}.

Calculation of the probability of an agglomerated particle breakup by impaction

The probability of breakup of the agglomerated particles by impaction depended on the frequency of the impaction, the impaction energy, particle sizes, the threshold energy of the break-up and the break-up resistance of the parameter for each material (Equation (1))[30].

$$P = 1 - e^{-f_{mat}dk(W_m - W_{m,\,min})} \qquad (1)$$

$W_{m,\mathrm{min}} =$ Threshold energy of break-up
$W_m =$ Impact energy
$d =$ particles diameter

f_{mat} = break-up resistance parameter
k = impact frequency

Since the material parameters; $W_{m,min}$ and f_{mat} in this simulation were constant, Equation (1)was simplified by neglecting the threshold energy of the break-up and the break-up resistance parameters (Equation (2)).

$$P = 1 - e^{-dkW_m} \qquad (2)$$

The aerosol dispersion experiment

Ventolin Rotacaps[®] (GlaxoSmithKline plc., Brentford, England) was used as it had been for the commercially available model drug. Each capsule of Ventolin Rotacaps[®] consisted of 200 µg of salbutamol sulfate with 25 mg of lactose[31]. The salbutamol sulfate to lactose ratio was 1:50 w/w. The Ventolin Rotacaps[®] were placed in the capsule chamber or the capsule port of the device and pierced with a needle making holes or a separate capsule body from the cap as in the Rotahaler[®]. The drug deposition was evaluated using the 8-stage Andersen Cascade Impactor (ACI; Copley Scientific Limited, Nottingham, UK). The particle collection plates were coated with silicone oil. The dispersion was operated at 60 LPM for 10 s to ensure that all the powder was released from the capsule. The evaluation of the dispersion at 60 LPM was for 10 s. This was due to the low resistance of the device (about 3 $(mbar)^{1/2}/(LPM))^{19}$. If the device was performed for 4 s, a high variation of the data was obtained. The operating relative humidity was controlled at 50 ± 5%. The ACI stages in this experiment were stages −1 to 6. The amount of drug deposited on each collection plate in each stage was eluted with water and diluted with an appropriate volume of mobile phase. The salbutamol sulfate content was analyzed using the HPLC technique as explained in the next subheading.

The FPF and the MMAD were calculated according to the United States Pharmacopeia[7]. The MMAD and %FPF were used to determine the performance of the drug delivery. The percent Emission (%EM) was calculated from the percentage of the drug emitted from the device.

Analysis of the salbutamol sulfate content

The salbutamol sulfate was analyzed by the high-performance liquid chromatography (Waters Corporation; Milford, MA) equipped with a fluorescence detector. The stationary phase was a C18 ACE 5 C18-AR 150 × 4.6 mm column (Advanced Chromatography Technologies Ltd; Aberdeen, Scotland). The mobile phase was 75:25 methanol:water with 1 g/L sodium dodecyl sulfate mobile phase using a flow-rate of 1 mL/min. The analytical excitation wavelength was 218 nm and the emission wavelength was 309 nm.

Result and discussion

The inhaler device model

The designed DPI was based on a single unit dose device, in which the dry powder medication was prefilled in a capsule. The design was based on commercially available devices, such as Rotahaler[®] and Cyclohaler[®]. The Rotahaler[®] was a low pressure drop device that a patient could operate with little effort but this suffered from having a low performance and a high variation in the dosage[32]. The Cyclohaler[®] was a medium pressure drop device. It generated a moderate dose of fine particles but had a comparatively low performance when compared to the new generation inhalers such as the Easyhaler[®], Neohaler[®], Breezehaler[®][33,34]. Thus, a design that was a combination of the Rotahaler[®] and Cyclohaler[®] was proposed with a low-pressure

drop and a high-performance device. Figure 2(A) illustrates the Cyclohaler[®], a commercially available inhaler device. Figure 2(B–D) shows the newly designed inhaler devices, namely models 1–3, respectively. The DPI consisted of 4 major parts; a mouthpiece (1), grid (2), inhaler body (3) and inhaler base (4) (Figure 2A–D). The air inlet orifices were on the side of the inhaler base (Figure 2A–D, 5,6). The capsule introduction port in the model 2 and model 3 devices (Figure 2B, C-7) was placed between two air inlet orifices. The Cyclohaler[®] and model 3 device had a capsule chamber at the bottom (Figure 2A, D-7) where the capsule was pierced by sharp needles. The grid was placed near to the cyclone aerosol dispersion chamber in the Cyclohaler[®] and in the model 3 device. For the model 1 and 2 devices, the grid was placed near to the mouthpieces opening orifice. The reason for keeping the grid in the inhalers was to increase the turbulence and fine particle fractions[16].

Computational fluid dynamics

The airflow velocity in all models was in the range of 15–60 m/s. Every model produced a similar cyclonic flow pattern like in the Cyclohaler[®], as shown in Figure 3. The cyclonic flow was mainly localized in the inhaler base of the Cyclohaler[®]. The cyclonic flow was regulated by the grid to provide a more straight flow pattern along the mouthpiece (Figure 3A). The model 1 device generated a swirly flow around the inhaler base and body with a lower velocity than that obtained in the Cyclohaler[®], the model 2 and the model 3 devices. The outlet flow was slightly swirling after passing the grid (Figure 3B). The cyclonic flow was quite strong in both the inhaler base and the body in the model 2 device (Figure 3C). When the model 1 device was compared to the model 2 device, there was only one difference in the model 2 device that it had a narrower inhaler body than model 1 device and this led to a higher airflow rate and more swirling. The flow in the model 2 device mouthpieces was nearly identical to that of the model 1 device due to both having a similar grid design and position. The model 3 device also produced a swirly flow at the inhaler base (Figure 3D). However the gird in the model 3 device, still produced turbulence. This phenomenon confirmed the previous investigation that the grid structure straightened the airflow before exiting the inhaler mouthpiece[16]. The grid area in the Cyclohaler[®] was 52 mm^2 and 128 mm^2 in model 1, 2 and 3 devices. The inhaler body cross sectional area in the Cyclohaler[®] and model 2 device was 95 mm^2 while in the model 1 and model 3 devices it was 452 mm^2, respectively. The grid void space had a direct effect on the flow velocity that was passing through the grid and as the grid area decreased the flow velocity increased. It was observed that a small grid area had a stronger flow straightening effect than a large grid area.

The pressure drop across the Cyclohaler[®] and the model 2 device was around 16–19 mbar while the model 1 and model 3 devices had a relatively low-pressure drop of about 4 mbar at 60LPM. The pressure drop characteristics of the model 2 device and the Cyclohaler[®] were not much different because they had the same design. The model 1 and 3 devices had a larger inhaler body than the Cyclohaler[®] and the model 1 device had a lower pressure drop and showed the same pressure drop as the Rotahaler[®] at 60 LPM[19]. It also indicated that all the proposed designs would not require too much patient's inhalation effort to operate. The model 2 device was modified to a narrower inhaler body than the model 1 device while the inhaler base, grid and mouthpiece were not changed and this resulted in a substantial increase in the pressure drop from 4 to 16 mbar at 60 LPM. The model 3 device had the same base design as the model 1 device except for the grid position and an additional capsule chamber. The auxiliary capsule chamber was attached to the bottom of the inhaler base.
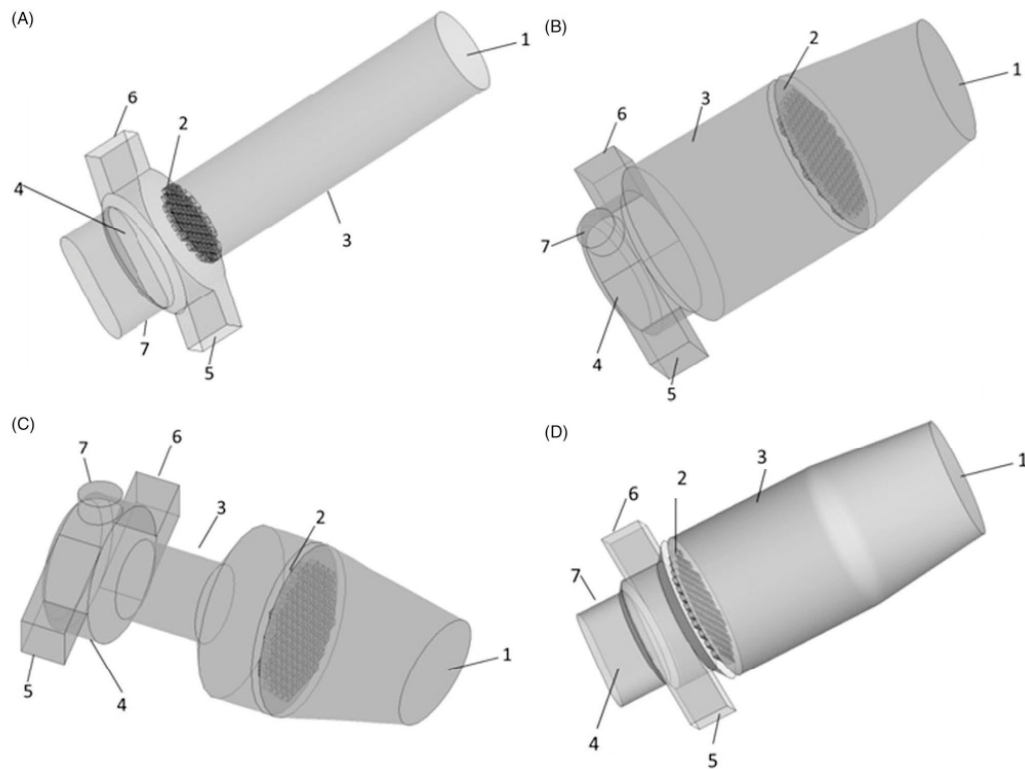
Figure 2. Internal dimension of the Cyclohaler® (A), model 1 (B), model 2 (C) and model 3(D).

Both models expressed the same pressure drop because the capsule chamber attachment was not involved in the flow path and the grid had the same void area.

The aerosol dispersion depended on both the impaction on the particle-device wall and the fluid dynamic shear force. The deagglomeration that occurred on the particle-device wall was based on the impaction frequency and the impaction kinetic energy (derived from the velocity of the particles upon impaction). The impaction events per particle of model 1, 2 and 3 devices were significantly higher than for the Cyclohaler® ($p = 0.000$) while there was no statistical difference between model 1 and model 2 devices ($p > 0.05$). The model 3 device produced the highest impaction events per particle (Table 2). This indicated that all the new designs created more frequent impactions on the device wall. The impaction energy in the Cyclohaler® was slightly higher than for the model 2 and model 3 devices but both were higher than for the model 1 device (Table 1). The model 1 device had the lowest impaction kinetic energy of the three new design models while the model 2 and 3 devices had the same impaction energy. It was observed that the narrowest channel in the flow path and the grid position had some relation to the impaction kinetic energy. The impaction kinetic energy and particle-wall impaction event were higher when the grid was placed near to the inhaler base. This was due to a high swirly airflow and a rapid change of direction. A narrow flow path also increased the impaction kinetic energy as it accelerated the particle velocity. This emphasized the importance of the grid in the inhaler design as previously discussed by Coates et al[16].

The breakup of the particle agglomerates by impaction was determined by the impaction frequency and the impaction energy[35]. The probability of deagglomeration by impaction was significantly different in each of inhaler designs. The model 3 device had the best deagglomeration potential compared to the Cyclohaler®, the model 1 and the model 2 devices. When a device with a similar kinetic energy was considered, it was found that the impaction frequency played an important role in the probability of deagglomeration.

The integral scale strain rate (ISSR) was chosen to represent the fluid dynamic shear force parameter. The ISSR is a ratio of the rate of dissipation of the turbulence and the rate and turbulence of the kinetic energy[27]. It was a measure of the velocity gradient across the integral scale eddies. The ISSR ranged from 1500 to $3300 \, \text{s}^{-1}$ and was dependent on the grid position. As the grid was placed nearer the mouthpiece the ISSR ranged from 1500 to 2000 in the model 1 and 2 devices. The grid was placed on top of the inhaler base in the Cyclohaler® and the model 3 device, in both cases the ISSR ranged from 2500 to 3300 and the grid area in the model 3 device was larger than the Cyclohaler® therefore the increase in the grid area reduced the ISSR. The Cyclohaler® exhibited the highest ISSR among the 4 inhalers. The peaks for the ISSR were 86 586, 59 521, 28 368 and 46 383 for the Cyclohaler®, and the model 1, 2 and 3 devices, respectively. Although the Cyclohaler® cannot produce much particle-wall impaction events and the probability of deagglomeration by impaction, the turbulent effect was high with either an average or peak ISSR. The model 3 device has a slightly lower turbulent
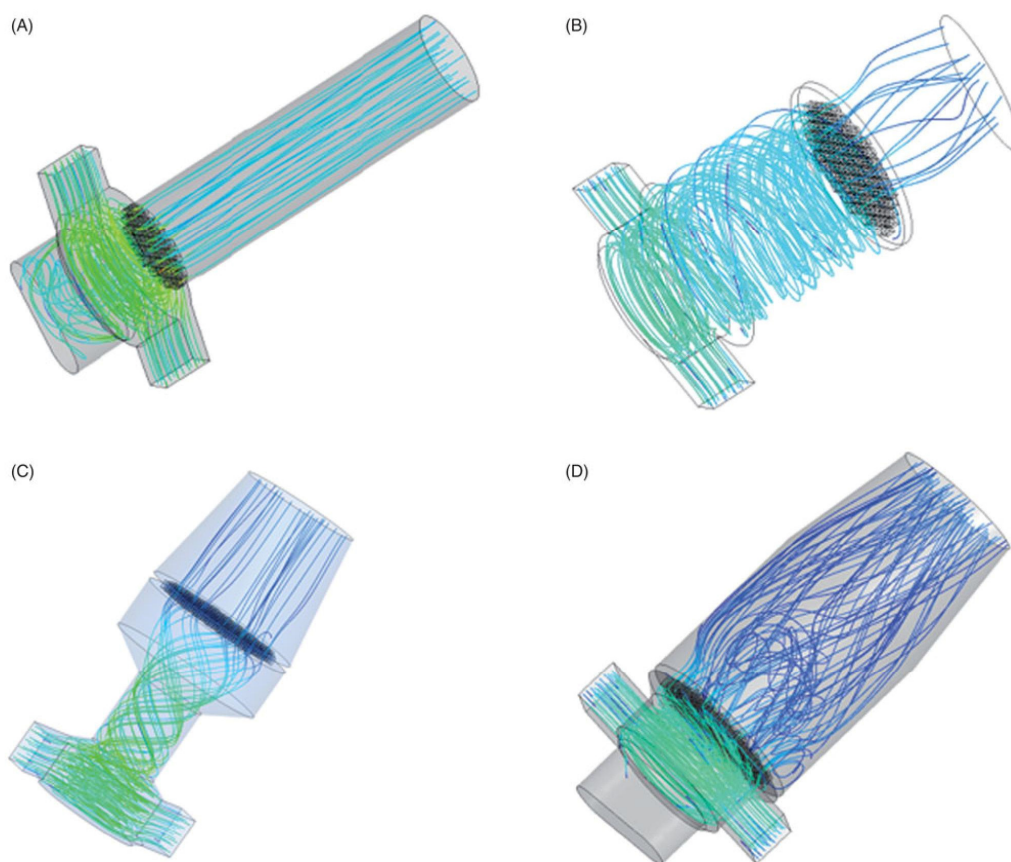
Figure 3. Velocity streamline of the Cyclohaler® (A), CAD model 1 (B), model 2 (C) and model 3 (D) at 60 LPM.

Table 1. Integral scale strain rate, impaction event per particle and peak impaction energy on the Cyclohaler® and models 1–3 at a flow rate of 60 LPM (mean ± SD, $n = 5$).

Model	Pressure drop (mbar)	Mean ISSR [peak] (s^{-1})	Impaction event per particle	Impaction Energy (m^2s^{-2})	Probability of impaction deagglomeration
Cyclohaler®	19	3316 [86 586]	107 ± 10	33.33 ± 3.63	0.10 ± 0.01
Model 1	4	1592 [59 521]	752 ± 122	18.80 ± 2.69	0.39 ± 0.06
Model 2	16	2037 [28 368]	760 ± 123	28.13 ± 2.07	0.52 ± 0.04
Model 3	4	2565 [46 383]	1723 ± 107	26.02 ± 1.23	0.69 ± 0.13

magnitude than that of the Cyclohaler® although it had the highest probability of generating the highest deagglomeration by impaction. These results supported the previous investigation that used CFD-DEM coupling to investigate the aerosolization mechanism and concluded that particle–wall impactions inside the inhaler chamber was a major breakage mechanism in the aerosolization process while interactions of the fluid particles in term of the ISSR may also have an effect on the generation of the fine aerosol particles in a carrier-based system[27]. In this case, there is a need to be a further investigation on the ISSR threshold that can detach drug particles from the carrier surface.

Performance *of in vitro* aerosol dispersion

Assessment of the *in vitro* aerosol dispersion indicated that all devices generated suitable respirable particles sizes with MMADs of around 2.8–3.9 µm (Figure 4B). The model 3 device produced the smallest MMAD (2.8 µm) and this was correlated with a relatively high *in silico* probability to predict the deagglomeration by impaction. This indicated that the model 3 device had a high ability to deagglomerate the dry powder formulations. The FPFs were 35.1 ± 2.3, 23.1 ± 2.3, 36.1 ± 2.8 and 49.5 ± 1.0 for the Cyclohaler®, the model 1, model 2 and model 3 devices, respectively (Figure 4A). The %FPF in the Cyclohaler®

Table 2. ANOVA with Tukey's honest significant difference test of an impaction event per particle.

Device	p Value		
	Impaction events per particle	Impaction kinetic energy	Probability of impaction deagglomeration
Cyclohaler®			
Model 1	0.000	0.006	0.000
Model 2	0.000	0.000	0.000
Model 3	0.000	0.000	0.000
Model 1			
Cyclohaler®	0.000	0.006	0.000
Model 2	0.999	0.000	0.031
Model 3	0.000	0.000	0.000
Model 2			
Cyclohaler®	0.000	0.000	0.000
Model 1	0.999	0.000	0.031
Model 3	0.000	0.365	0.007
Model 3			
Cyclohaler®	0.000	0.000	0.000
Model 1	0.000	0.000	0.000
Model 2	0.000	0.365	0.007

The mean difference was significant at the 0.05 level.

Table 3. Drug retentions in the capsule of the Cyclohaler® and model 1, 2 and 3 devices (mean ± SD, $n = 3$).

Device	Capsule retention (µg)
Cyclohaler®	19.74 ± 0.05
Model 1	27.07 ± 1.92
Model 2	27.40 ± 2.27
Model 3	17.82 ± 0.26

Cyclohaler®. The poor relationship of the Cyclohaler® to the %FPF and the probability of predicted deagglomeration by impaction may be caused by the effect of the related deagglomeration in the capsule that was not included in the computational simulation and the strong turbulence in the Cyclohaler® that was observed in both the average and peak ISSR that could assist deagglomeration of the particles. The peak ISSR in the Cyclohaler® was far higher than occurred in the model 1, 2 and 3 devices. Although previous findings in a carrier free DPI system had indicated that the turbulent flow was not strong enough to overcome the strength of agglomeration, in the carrier-based system it would be different[27]. It was highly dependent on the design of the inhalers[37]. The turbulence played some roles in the dispersion of the aerosol in the experimental rigs. In this case, in the Cyclohaler® the turbulence was more dominant than in the other inhalers tested in this study. The multiple regressions of the ISSR and the probability of deagglomeration by impaction (P_{deagg}) revealed that the both parameters had a similar significant level on the %FPF at p value 0.041 and 0.039, respectively. The linear equation from the multiple regressions is in Equation (3) with correlation coefficient of 0.9985. This evidence supported the importance of the turbulent factor and the mechanical impaction factor on the generation of fine particles. The Equation (3) could be used as a guideline to develop further Cyclohaler® derived DPIs.

$$\%\text{FPF} - 0.014(\text{ISSR}) + 42.681(P_{deagg}) - 15.194 \qquad (3)$$

The retention of salbutamol sulfate in the capsule by all devices was 18–27 µg (5–7%) of the nominal dose. This indicated that there was no problem in the process of emptying the capsule in the model 1 and 2 devices and each of them showed a slightly higher drug retention in the capsule than the Cyclohaler® and the model 3 devices. There were no significant differences in the %FPF between the Cyclohaler® and the model 2 devices (Table 3). The model 1 and model 2 devices had the same capsule introduction method. The capsule cap and body would be pulled apart and only the capsule body with the powder was put in the inhaler while the cap was still in the capsule port. The air stream caused vigorously shaking the capsule body, while emptying the drug content.

Conclusion

In conclusion, three modifications of the Cyclohaler® were designed and tested by CFD simulation to examine their potential for use as higher performance inhaler devices. Modification of the Cyclohaler® did produce differences in the performance of the devices. The model 3 device had a good performance that allowed for prediction of the probability of deagglomeration. The experimental result indicated that the model 3 device had a good aerosolization performance and this was confirmed by the CFD result. It can generate up to 50% FPF and had a low MMAD when operated at 60 LPM with the Ventolin Rotacaps®. Further mechanical modifications, such as to the capsule piercing

Figure 4. %FPF (A) and MMAD (B) of the Cyclohaler®, and model 1, 2 and 3 devices. Data are presented as a mean ± SD, $n = 3$.

confirmed the work of Parisini el al. and was about 33% FPF[36]. The %FPF was highest in the model 3 device and that was the same trend as for the prediction of the probability of deagglomeration by impaction. The Cyclohaler® and the model 2 devices had a similar %FPF due to the base design that was closely related even though the capsule insertion method and grid position were different. The %FPF in the model 1 device was only about 23%, the lowest of the 4 devices while it had a higher probability of predicted deagglomeration by impaction than the

mechanism and for the inhaler base–body connection had to be refined for practical use. The inhaler design in the Cyclohaler®-type device was highly dependent on the grid position. Placing the grid near to the turbulence-generating chamber did improve the aerosolization performance. The pressure drop of the device had little effect on the dispersal of the aerosol.

Declaration of interest

References

1. Balducci AG, Cagnani S, Sonvico F, et al. Pure insulin highly respirable powders for inhalation. Eur J Pharm Sci. 2014;51:110–117.
2. Finlay WH. The mechanics of inhaled pharmaceutical aerosols. London: Academic Press; 2001.
3. Telko MJ, Hickey AJ. Dry powder inhaler formulation. Resp Care 2005;50:1209–1227.
4. Steckel H, Markefka P, teWierik H, Kammelar R. Effect of milling and sieving on functionality of dry powder inhalation products. Int J Pharm 2006;309:51–19.
5. Frijlink H, De-Boer A. Dry powder inhalers for pulmonary drug delivery. Exprt Opin Drug Deliv 2004;1:67–86.
6. Mitchell JP, Nagel MW. Improved laboratory test methods for orally inhaled products. Ther Deliv 2013;4:1003–1026.
7. United States Pharmacopeia Convention. <601> Aerosol, nasal sprays, metered-dose inhalers, and dry powder inhalers. United States Pharmacopeia and National Formulary (USP 34-NF 29). 1. Rockville, MD: United States Pharmacopeia Convention; 2011:219–39.
8. Daniher DI, Zhu J. Dry powder platform for pulmonary drug delivery. Particuology 2008;6:225–238.
9. Islam N, Gladki E. Dry powder inhalers (DPIs)—a review of device reliability and innovation. Int J Pharm 2008;360:1–11.
10. Islam N, Cleary MJ. Developing an efficient and reliable dry powder inhaler for pulmonary drug delivery – a review for multidisciplinary researchers. Med Eng Phys 2012;34:409–427.
11. Desai SS, Aher AA, Kadaskar PT. Methods for reduction of cohesive forces between carrier and drug in DPI formulation. Drug Dev Ind Pharm 2013;39:1589–1598.
12. Coates MS, Chan H-K, Fletcher DF, Raper JA. Influence of air flow on the performance of a dry powder inhaler using computational and experimental analyses. Pharm Res 2005;22:1445–1453.
13. Zhou QT, Tang P, Leung SSY, et al. Emerging inhalation aerosol devices and strategies: where are we headed? Adv Drug Deliv Rev 2014;75:3–17.
14. Coates MS, Chan HK, Fletcher DF, Chiou H. Influence of mouthpiece geometry on the aerosol delivery performance of a dry powder inhaler. Pharm Res 2007;24:1450–1456.
15. Coates MS, Chan HK, Fletcher DF, Raper JA. Effect of design on the performance of a dry powder inhaler using computational fluid dynamics. Part 2: air inlet size. J Pharm Sci 2006;95:1382–1392.
16. Coates MS, Fletcher DF, Chan HK, Raper JA. Effect of design on the performance of a dry powder inhaler using computational fluid dynamics. Part 1: grid structure and mouthpiece length. J Pharm Sci 2004;93:2863–2876.
17. Wong W, Fletcher DF, Traini D, et al. Particle aerosolisation and break-up in dry powder inhalers 1: evaluation and modelling of venturi effects for agglomerated systems. Pharm Res 2010;27:1367–1376.
18. Smith IJ, Parry-Billings M. The inhalers of the future? A review of dry powder devices on the market today. Pulm Pharmacol Ther 2003;16:79–95.
19. Srichana T, Martin GP, Marriott C. Dry powder inhalers: the influence of device resistance and powder formulation on drug and lactose deposition in vitro. Eur J Pharm Sci 1998;7:73–80.
20. Elkins MR, Robinson P, Anderson SD, et al. Inspiratory flows and volumes in subjects with cystic fibrosis using a new dry powder inhaler device. Open Resp Med J 2014;8:1–7.
21. Chew N, Chan H. In vitro aerosol performance and dose uniformity between the Foradile Aerolizer and the Oxis Turbuhaler. J Aerosol Med 2001;14:495–501.
22. Zainudin B, Biddiscombe M, Tolfree S, et al. Comparison of bronchodilator responses and deposition patterns of salbutamol inhaled from a pressurised metered dose inhaler, as a dry powder, and as a nebulised solution. Thorax 1990;45:469–473.
23. Richards R, Dickson C, Renwick A, et al. Absorption and disposition kinetics of cromolyn sodium and the influence of inhalation technique. J Pharmacol Exp Ther 1987;241:1028–1032.
24. Borgstrom L, Newman S, Weisz A, Moren F. Pulmonary deposition of inhaled terbutaline: comparison of scanning gamma camera and urinary excretion methods. J Pharm Sci 1992;81:753–755.
25. Thornton C, Liu L. How do agglomerates break. Powder Technol 2004;143–144:110–116.
26. Guo Y, Kafui KD, Wu C-Y, et al. A coupled DEM/CFD analysis of the effect of air on powder flow during die filling. AIChE J 2003;55:49–62.
27. Tong Z, Zheng B, Yang R, et al. CFD-DEM investigation of the dispersion mechanisms in commercial dry powder inhalers. Powder Technol 2013;240:19–24.
28. Hoppentocht M, Hagedoorn P, Frijlink HW, Boer AHd. Technological and practical challenges of dry powder inhalers and formulations. Adv Drug Deliv Rev 2014;75:18–31.
29. Oliveira RF, Teixeira SFCF, Silva LF, et al. Development of new spacer device geometry: a CFD study (Part I). Comput Method Biomech 2012;15:825–833.
30. Vogel L, Peukert W. Breakage behaviour of different materials—construction of a mastercurve for the breakage probability. Powder Technol 2002;129:101–111.
31. Adams WP, Lee SL, Plourde R, et al. Effects of device and formulation on in vitro performance of dry powder inhalers. AAPS J 2012;14:400–409.
32. Vidgren M, Paronen P, Vidgren P, et al. In vivo evaluation of the new multiple dose powder inhaler and the Rotahaler using gamma scintigraphy. Acta Pharm Nordica 1990;2:3–10.
33. Pavkov R, Mueller S, Fiebich K, et al. Characteristics of a capsule based dry powder inhaler for the delivery of indacaterol. Curr Med Res Opin 2010;26:2527–2533.
34. Selroos O. Dry-powder inhalers in acute asthma. Ther Deliv 2014;5:69–81.
35. Ruzycki CA, Javaheri E, Finlay WH. The use of computational fluid dynamics in inhaler design. Expert Opin Drug Deliv 2013;10:307–333.
36. Parisini I, Cheng SJ, Symons DD, Murnane D. Potential of a cyclone prototype spacer to improve in vitro dry powder delivery. Pharm Res 2014;31:1133–1145.
37. Voss A, Finlay WH. Deagglomeration of dry powder pharmaceutical aerosols. Int J Pharm 2002;248:39–50.

Proceedings 1

Aerodynamics Study in Dry Powder Inhalers Using Computational Fluid Dynamics

(Manuscript submit to *the 2nd Current Drug Development International Conference, 2-4 May 2012 Phuket, Thailand.*)

Aerodynamics Study in Dry Powder Inhalers Using Computational Fluid Dynamics

Tan Suwandecha[1], Teerapol Srichana[2]

[1]Faculty of Pharmaceutical Sciences, Prince of Songkla University, Songkhla, Thailand.
[2]Drug Delivery Research Excellent Center, Faculty of Pharmaceutical Sciences, Prince of Songkla Univesity, Songkhla, Thailand.
E-mail address: teerapol.s@psu.ac.th

Abstract- Dry powder inhalers (DPIs) have been extensively used for delivering medication to the lungs. The different designs of DPI device affect the particles aerosolization processes. The processes are not observable in experiment thus computational fluid dynamics can allow us to investigate air-flow field, turbulence kinetics energy and the device resistance. In this research, we used the Cyclohaler® and Inhalator® devices as models for computational simulation. The device resistant, the velocity vector, velocity contour and the turbulence kinetic energy (TKE) were observed. The Cyclohaler® was a medium resistance device while the Inhalator® had high resistance related to their geometries. The TKE directly relates to the flow-rate. The TKE in the Cyclohaler® is lower than that in the Inhalator® due to narrow geometry resulting in a high velocity air-flow. In short, maximizing the turbulence and the kinetic energy by adding a grid and a cyclone-like design were key factors to achieve high deagglomeration of the particles.

Introduction

Dry powder inhalers (DPIs) have been extensively used for delivering medication to the lungs. Available DPI devices have various designs for such as mouthpieces, air inlet channels and design of chambers that lead to differences in the aerodynamic characteristics [1-3]. A major aerodynamic characteristic is the resistance of the device that affects the degree of turbulence and shear force in the device [4]. In this case, high resistant devices usually provide a high degree of turbulence and shear force but can cause difficulty for asthmatic patients who have a limited inhalation force [5]. The level of turbulence is influenced by air inlet channel while the design of the mouthpieces controls the outlet air velocity and flow pattern [6]. The velocity of the outlet air and flow pattern from the device to oral cavity can cause drug loss in the oropharyngeal region by inertial impactions. One study has indicated that the optimization of how the magnitude of the turbulence maximized the dispersion capability of DPIs, whereas the in-deep mechanism is still unclear.

The formulation of DPIs usually employs lactose as the bulk carrier with only a few milligrams of drug[7]. Drug particles loosely attach on the surface of lactose carrier. During the aerosolization process, the drug particles are detaches from the carrier surface if energy from fluid shear overcomes the adhesion forces between drug-carrier particles [8, 9]. The large carrier particles deposit on the upper airways, whereas the smaller drug particles reach the lower part of the lungs [10].

Computational fluid dynamics (CFD) is used in engineering fields and is now also gaining popularity in pharmaceutical research. It is useful for investigating aerodynamic parameters such as tge turbulence kinetics energy, pressure and aerodynamics shear force and the trajectory of particles. These parameters allow us to better understand the aerosolization processes in the DPI devices than any in vitro experiment.
The aims of this research were to investigate the turbulence kinetic energy and device resistance during the aerosolization processes in DPI devices.

Materials and Methods

1) Measurements of the dimensions and pressure drop of the devices: The inhaler device dimensions were measured using a Vernier caliper and the obtained data were used to compare between devices. The internal resistance of the DPI device was determined using an in house designed apparatus. The apparatus consisted of a metal box, approximately 10 cm^2, with a Perspex cover housing the device (Fig. 1). The device was held between two Teflon ring seals. One side of the box was connected to a pump. Air flow was drawn through the apparatus at various flow-rates by adjusting a rotameter (Fig. 1). The pressure drop across the apparatus containing device was recorded by a digital manometer (Extech®, Waltham, MA, USA). The difference in the pressure drop, was determined with and without the device in place and was defined as the specific pressure drop of that device at a particular flow rate. The device resistance was calculated using the pressure drop and the flow-rate as shown in Equation 1. The square root of the pressure drop versus the flow rate on the x-axis was plotted; the slope from the graph is the specific resistance of the device (R_D).
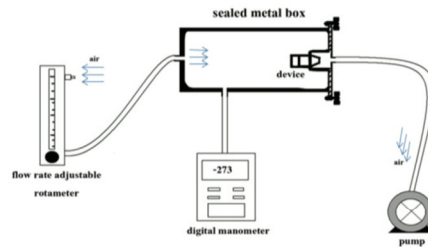
Figure 1 Resistance device measurement apparatus

$$\sqrt{\Delta P_D} = R_D Q \qquad \qquad \text{Equation 1}$$

P_D = the pressure drop across the device (mbar)
R_D = the specific resistance of the device (mbar)$^{1/2}$/(Lpm)
Q = flow rate (Lpm)

2) Computational Simulation: The dimensions of the Cyclohaler® and Inhlalator® devices were precisely measured using a Vernier caliper. A 3D model of the DPIs devices was created using Gambit® software (ANSYS, Inc., USA). The 3D models were meshed to create computational nodes. Mesh quality was controlled using the equiskewness parameter that determines the deviation of the mesh shape from the hexagonal or tetrahedral shape. CFD problems were solved using the finite volume method and the Fluent® software package (ANSYS, Inc., USA). The fluid dynamic solving was based on momentum, mass and energy conservation (Navier-Stoke equation) and CFD is repeated until the residue error was less than 1×10^{-6}. Post-processing of CFD simulation was analyzed in the following properties.

2.1. Pressure drop across device and device resistance: The simulation setup for the pressure drop was carried out at 20-90 Lpm for both inhaler models and the pressure drop was calculated to obtain the resistance of the device using equation 1. The resistance of the device was validated with an experimental result to ensure that the inhaler models and simulation parameters were set appropriately.

2.2. Velocity vector and velocity contour and turbulence kinetic energy (TKE): The velocity vector and velocity contour and turbulence kinetic energy were plotted to visualize the flow characteristics in the inhalers device.

Results and discussion

1) Measurement of device resizstant: The device resistance from the experiment and the CFD simulation of the Inhalator® and Cyclohaler® was well correlated. The Cyclohaler® was a medium resistance device while the Inhalator® had high resistance [11]. From fluid the dynamics theory resistance to the flow in the tube directly related to the channel cross sectional area [12]. The device resistances of the Inhalator® and Cyclohaler® from the experiment were 0.1837 and 0.0753 units, respectively (Table 1). The Inhalator® had a 3.1×10^{-4} m^2 narrowest channel cross sectional area at the inlet while Cyclohaler® had a 6.7×10^{-5} m^2 narrowest cross sectional area at inlet. The narrowest cross sectional area largely affects the device resistance. It confirmed that the Cyclohaler® had a lower resistance than that of the Inhalator® due to the Cyclohaler total inlet cross sectional being about 5-times larger than the Inhalator®.

Table 1 Inhalator® and Cyclohaler® device dimension and device resistance

Device	Total inlet surface area (m^2)	Total outlet surface area (m^2)	Device resistance (mbar$^{1/2}$·min /L)	
			CFD	Experiment
Inhalator®	7.3×10^{-6}	3.1×10^{-4}	0.1837	0.1975
Cyclohaler®	6.7×10^{-5}	8.0×10^{-5}	0.0753	0.0801

2) Computational Simulation
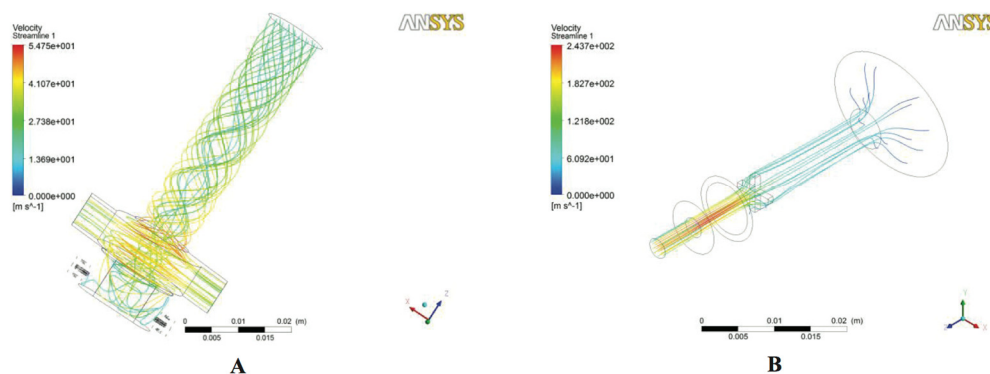
Figure 2 Geometry and Velocity streamline of Cyclohaler® (A) and Inhalator® (B) at 90Lpm

Figure 2 A shows that the Cyclohaler® is a unit-dose dry powder inhaler device. The Cyclohaler® consists of three parts that were mouthpiece tube, cyclone chamber and capsule holder. Medication powder was filled into a capsule and put in the capsule holder at the bottom of the device. The press button on the device was used to release needles to pierce holes on the capsule. Dry powder was then released through the holes. After that the patient inhaled the medication through the mouthpiece. During inhalation the medication powder is dispersed and aerosolized along the device.

The Inhalator® (Figure 2B) is also a unit-dose device which has a relatively simple design being a straight tube with an eclipse bell-shape mouthpiece. The medication capsule holder is in the lower part of the device. The grid is located between the straight tube part and the conical part.

The velocity streamline of the Cyclohaler® and Inhalator® were a visualized air-flow profile in the Cyclohaler and Inhalator (Figure 2). In the Cyclohaler®, the flow had input from eight small holes at the rear of the device and two auxiliary inlets on the side of the cyclone chamber (Figure 2A). The auxiliary inlet is configured in a tangent from to create a cyclone like effect and make a swirly flow in the cyclone chamber with velocity of 4-5.5 m/s. The airflow was transitioned to the mouthpiece tube that decreased the velocity to $1.37 - 2.8$ m/s. The flow entered the Inhalator® device at a small inlet tube and changed direction when passing the cross grid (Figure 2B). The air-flow velocity was very high at the beginning (206 - 212 m/s) then decreased along the device to mouthpiece (4 - 5 m/s).

The turbulence kinetic energy (TKE) is the mean kinetic energy per unit mass associated with eddies in the turbulent flow. Physically, the TKE is characterized by the measured root-mean-square (RMS) velocity fluctuations. TKE is directly related to the magnitude of the turbulence [13] . The TKE in the Cyclohaler® ranges from 4-17 m^2/s^2, 12-85 m^2/s^2 and 27-220 m^2/s^2 at a flow-rate 30, 60 and 90 LPM, respectively. At the flow-rate of 30 LPM, TKE is quite low compared to that at 60 and 90 LPM. TKE occurs mostly at the inlet and cyclone part of the Cyclohaler® due to the rapid change of airflow direction and airflow velocity as visualized in the velocity streamline and contour plot of the TKE. In this case an increasing of the TKE elevates the level of particle impaction because of the rapidly swirling of the airflow in the cyclone part of the device that introduces a greater probability of impaction of the on the-wall.

For the Inhalator® the TKE were 2-242 m^2/s^2, 7.3-969 m^2/s^2 and 1.45 – 2123 m^2/s^2 at the flow-rates of 30, 60 and 90 LPM, respectively. The magnitude of the TKE in the Inhalator® was about 10 times higher than in the Cyclohaler®. The TKE mainly occurred around the cross grid where the air-flow changed its direction. The TKE also indicates the amount of energy that fluid interacts with the particles and causes fluid dynamic shearing on the particles. More fluid shearing on the carrier-drug particle agglomerates so increase the probability of drug particles detachment from carrier surface. According to work of Voss et.al. 2002, turbulence plays a key role in the aerosolization process [14]. Thus, the Inhalator® has a higher probability of detachment of the drug particles from the carrier surface than the Cyclohaler® as determined by fluid dynamic shearing.

Conclusion

In summary, the Cyclohaler® and Inhalator® are medium and low resistant device. Cyclohaler® used cyclone-like design that consists of tangential flow cross the axial flow. It leads to swirly airflow that means more turbulence kinetic energy in the flow. TKE can shear up particle agglomerate apart. In contrast, Inhalator® has straight tube design and grid. The grid obstructs some air-flow, so the air and particle rapidly change it direction. The high

resistance of the Inhalator$^®$ maximizes the air velocity is the cause of energetic shear. However, the inertial impact to airways of high velocity particles will cause drug loss. The device performance needs experimental evaluation to verify relationship with CFD in future work.

Acknowledgement

References

[1]   Coates, M.S., et al. (2007) Influence of mouthpiece geometry on the aerosol delivery performance of a dry powder inhaler. Pharm Res. 24(8):1450-1456.
[2]   Coates, M.S., et al. (2006) Effect of design on the performance of a dry powder inhaler using computational fluid dynamics. Part 2: Air inlet size. J Pharm Sci. 95(6):1382-1392.
[3]   Coates, M.S., et al. (2004) Effect of design on the performance of a dry powder inhaler using computational fluid dynamics. Part 1: Grid structure and mouthpiece length. J Pharm Sci. 93(11):2863-2876.
[4]   Selvam, P., et al. (2010) A novel dry powder inhaler: Effect of device design on dispersion performance. Int J Pharm. 401(1–2):1-6.
[5]   Lee, S., et al. (2009) In Vitro Considerations to Support Bioequivalence of Locally Acting Drugs in Dry Powder Inhalers for Lung Diseases. APPS J. 11(3):414-423.
[6]   Gac, J., T.R. Sosnowski, and L. Gradon (2008) Turbulent flow energy for aerosolization of powder particles. J. Aerosol. Sci. 39(2):113-126.
[7]   Daniher, D.I. and J. Zhu (2008) Dry powder platform for pulmonary drug delivery. Particuology. 6(4):225-238.
[8]   Begat, P., et al. (2004) The Cohesive-Adhesive Balances in Dry Powder Inhaler Formulations II: Influence on Fine Particle Delivery Characteristics. Pharm Res. 21(12):1826-1833.
[9]   Calvert, G., M. Ghadiri, and R. Tweedie (2009) Aerodynamic dispersion of cohesive powders: A review of understanding and technology. Adv Powder Thechnol. 20:4-6.
[10] Zhou, Y. and Y.S. Cheng (2000) Particle deposition in first three generations of a human lung cast. J. Aerosol. Sci. 31(Supplement 1):140-141.
[11] Srichana, T., G.P. Martin, and C. Marriott (1998) Dry powder inhalers: The influence of device resistance and powder formulation on drug and lactose deposition in vitro. Eur J Pharm Sci. 7(1):73-80.
[12] White, F.M., Fluid Mechanics. 4th ed2001, New York: McGraw-Hill.
[13] George, W.K., Lectures in Turbulence for the 21st Century2005, Göteborg, Sweden: Department of Thermo and Fluid Engineering, Chalmers University of Technology.
[14] Voss, A. and W.H. Finlay (2002) Deagglomeration of dry powder pharmaceutical aerosols. Int. J. Pharm. 248(1-2):39-50.

VITAE

Name	Mr. Tan Suwandecha
Student ID	5110730002

Education Attainment

Degree	Name of Institution	Year of Graduation
Bachelor of Pharmacy	Prince of Songkla University	2008

Scholarship Awards during Enrollment

1. Thailand Research Fund through The Royal Golden Jubilee Ph.D. Program (PhD0025/2552)
2. Prince of Songkla University National Research University Project of Thailand Office of the Higher Education Commission.
3. Thesis Grant

    The Graduate School, Prince of Songkla University.
4. Thesis Grant

    The Nanotec-PSU Excellence Center on Drug Delivery System, Faculty of Pharmaceutical Sciences, Prince of Songkla University.
5. Conference Scholarship

    Faculty of Pharmaceutical Sciences, Prince of Songkla University.

List of Publication and Proceedings

Publication

1. **Suwandecha, T.**, Assawadarakorn, K., Srichana, T. 2012. Feasibility studies of using a tobacco pipe as a dry powder inhaler device. *Thai Journal of Pharmaceutical Science* 36:1-11
2. **Suwandecha, T.**, Wongpoowarak, W., Maliwan, K., Srichana, T. 2014. Effect of turbulent kinetic energy on dry powder inhaler performance. *Powder Technology* 267:381-391.

3. **Suwandecha, T.**, Wongpoowarak, W.,Srichana, T. Computer-aided design of dry powder inhalers using computational fluid dynamics to assess performance. *Pharmaceutical Development and Technology*. Manuscript accepted 05 September 2014

4. Sukasame, N., Nimnoo, N., **Suwandecha, T.**, Srichana, T.2011. Pharmacodynamics of dry powder formulations of salbutamol for delivery by inhalation *Asian Biomedicine* 5(4):475-483.
    (**Remark :** This paper is not related to Ph.D. Thesis)

5. Dechraksa, J., **Suwandecha, T.**, Maliwan, K., Srichana, T. 2014. The comparison of fluid dynamics parameters in an andersen cascade impactor equipped with and without a preseparator. *AAPS PharmSciTech* 15(3):792-801.
    (**Remark :** This paper is not related to Ph.D. Thesis)

Proceedings

1. **Suwandecha, T.,** Assawadarakorn, K., Srichana, T., 2009. Evaluation of tobacco pipe as dry powder inhaler device. The 6th Asian Aerosol Conference (AAC 2009), 24-27 November 2009. Bangkok, Thailand.

2. **Suwandecha, T.,** Srichana, T., 2012. Aerodynamics Study in Dry Powder Inhalers Using Computational Fluid Dynamics. The 2nd Current Drug Development International Conference, 2-4 May 2012 Phuket, Thailand.

3. **Suwandecha, T.,** Srichana, T., 2013. Fluid flow study in dry powder inhalers device. Inhalation Asia 2013 Pulmonary and Intranasal Drug Delivery Conference, 26-28 June 2013, The University of Hong Kong, China.

4. **Suwandecha, T.,** Srichana, T., 2014. Development of Simple Dry Powder Inhaler Device. The 3nd Current Drug Development International Conference, 1-3 May 2014, Pavilion Queen's Bay, Krabi, Thailand.